NAT'L INST. OF STAND & TECH
A11106 387727
NIST
PUBLICATIONS

NISTIR 6414

Characterization and Identification of Super-Effective Thermal Fire Extinguishing Agents—First Annual Report

William M. Pitts[1], Jiann C. Yang[1], Marcia L. Huber[2], and Linda G. Blevins[1]

[1]Building and Fire Research Laboratory
Gaithersburg, Maryland 20899

[2]Chemical Sciences and Technology Laboratory
Boulder, CO 80303

United States Department of Commerce
ology Administration
al Institute of Standards and Technology

NEXT GENERATION FIRE SUPPRESSION TECHNOLOGY PROGRAM

QC
100
.U56
NO.6414
19999

NISTIR 6414

Characterization and Identification of Super-Effective Thermal Fire Extinguishing Agents—First Annual Report

William M. Pitts[1], Jiann C. Yang[1], Marcia L. Huber[2], and Linda G. Blevins[1]

October 1999

[1]Building and Fire Research Laboratory
National Institute of Standards and Technology
Gaithersburg, MD 20899

[2]Chemical Sciences and Technology Laboratory
National Institute of Standards and Technology
Boulder, CO 80303

U.S. Department of Commerce
William M. Daley, *Secretary*
Technology Administration
Gary R. Bachula, *Acting Under Secretary for Technology*
National Institute of Standards and Technology
Raymond G. Kammer, *Director*

TABLE OF CONTENTS

LISTS OF TABLES iii

LISTS OF FIGURES iv

EXECUTIVE SUMMARY vii

I. INTRODUCTION 1

II. SCREENING OF THERMOPHYSICAL PROPERTIES DATABASES FOR SUPER EFFECTIVE THERMAL AGENTS 1

III. DETAILED CHEMICAL KINETIC MODELING OF EXTINGUISHMENT BEHAVIOR FOR THERMAL AGENTS IN METHANE/AIR DIFFUSION FLAMES 6

A. Introduction 6

B. Modeling Approach 13

C. Effects of Nitrogen Addition on Diffusion Flame Extinction and Extinguishment 21

D. Effects of Argon Addition on Extinction and Extinguishment of Methane Diffusion Flames Burning in Argon "Air" 24

E. Calculated Extinguishing Concentrations for Several Gaseous Thermal Agents 24

F. Effects of Dilution and Heat Extraction Location Relative to the Flame Front on Extinction and Extinguishment of Diffusion Flames 30

G. Prediction of Extinguishing Concentration for HFE7100 41

H. Discussion and Summary 43

IV. SURFACE COOLING 44

A. Introduction 44

B. Evaporation of Liquid Droplets 46

C. Spray Cooling 48

D. Convective Regime 50

E. Nucleate Boiling Regime 50

F. Critical Heat Flux 51

G. Transition and Film Boiling Regimes 52

H. Summary and Concluding Remarks 53

V. RECOMMENDATIONS FOR ADDITIONAL STUDY 54

VI. ACKNOWLEDGEMENTS 55

VII. REFERENCES 55

LIST OF TABLES

Table 1. Family Types in the DIPPR Database 2

Table 2. Results of Search for Compounds with High Heat of Vaporization at the Normal Boiling Point 4

Table 3. References for Property Data (Critical Point, Normal Boiling Point, Heat of Vaporization, Liquid Heat Capacity) 5

Table 4. Results of Search for Compounds with High Liquid Phase Heat Capacities at the Normal Boiling Point 6

Table 5. Results of Search for Compounds with High ΔH^{Total} (Molar Basis) 7

Table 6. Results of Search for Compounds with High ΔH^{Total} (Mass Basis) 8

Table 7. Some Parameters Used in Most Oppdif Calculations 16

Table 8. Various Measures of Strain Rate Calculated for the Methane/Air Diffusion Flame at Extinction 20

Table 9. Extinguishing Concentrations (Mole Fraction) of Thermal Agents 27

LIST OF FIGURES

Figure 1. Maximum flame temperature plotted as a function of the equal fuel and air velocity magnitudes for a methane/air opposed flow diffusion flame. 16

Figure 2. Calculated strain rates, a, are plotted as a function of distance from the fuel exit for low exit velocity magnitudes (25 cm/s for fuel and air) and for a condition very close to extinction (320.1 cm/s). 17

Figure 3. The maximum flame temperature is plotted against a characteristic local strain rate, $|a_o|$, defined to be equal to the highest absolute value of strain rate on the air side observed outside of the boundary layer associated with the flame. 18

Figure 4 Mixture fraction is plotted as a function of distance from the fuel exit for low exit velocity magnitudes (25 cm/s for fuel and air) and for a condition very close to extinction (320.1 cm/s). 18

Figure 5. Calculated scalar dissipation rates, χ, are plotted as a function of distance from the fuel exit for low exit velocity magnitudes (25 cm/s for fuel and air) and for a condition very close to extinction (320.1 cm/s). 19

Figure 6. Values of maximum flame temperature for opposed-flow methane/air diffusion flames are plotted as a function of χ_s which is varied by changing the velocities of the fuel and air. Extinction is calculated to occur for $\chi_s = 20.7\ s^{-1}$. 20

Figure 7. Maximum calculated flame temperatures are plotted against methane and oxidizer exit velocity magnitudes for a series of methane/air opposed flow diffusion flames diluted with nitrogen. Symbols correspond to the percentage of added nitrogen. 22

Figure 8. Ratios for the indicated measures of conditions at flame extinction are plotted as a function of the percentage of nitrogen added to the air for methane/air flames. 23

Figure 9. Maximum calculated flame temperatures are plotted against methane and oxidizer flow velocity magnitudes for a series of methane/argon "air" opposed flow diffusion flames diluted with argon. Symbols correspond to the percentage of added argon. 25

Figure 10. Maximum calculated flame temperatures are plotted against methane and oxidizer flow velocity magnitudes for a series of methane/air opposed flow diffusion flames diluted with argon. Symbols correspond to the percentage of added argon. 25

Figure 11. Maximum calculated flame temperatures are plotted against methane and oxidizer flow velocity magnitudes for a series of methane/air opposed flow diffusion flames diluted with helium. Symbols correspond to the percentage of added helium. 26

Figure 12. Maximum calculated flame temperatures are plotted against methane and oxidizer flow velocity magnitudes for a series of methane/air opposed flow diffusion flames diluted with carbon dioxide. Symbols correspond to the percentage of added carbon dioxide. 26

Figure 13. Maximum calculated flame temperatures are plotted against methane and oxidizer flow velocity magnitudes for a series of methane/air opposed flow diffusion flames diluted with water vapor. Symbols correspond to the percentage of added water vapor. 27

Figure 14. Values of maximum flame temperature at extinction are plotted as a function of the corresponding fuel and oxidizer velocity magnitudes for a range of concentrations of various thermal agents..... 29

Figure 15. Values of maximum flame temperature at extinction are plotted as a function of the corresponding global strain rates, a_g, for a range of concentrations of various thermal agents..... 29

Figure 16. Values of maximum flame temperature at extinction are plotted against the corresponding characteristic local strain rates, $|a_o|$, defined as the highest absolute value of strain rate observed outside of the boundary layer on the oxidizer side of the flame, for a range of concentrations of various thermal agents. 30

Figure 17. Maximum flame temperatures at extinction for N_2, Ar, He, and CO_2 as a function of the corresponding fuel and oxidizer velocity magnitudes are fit by two piecewise fourth order polynomials (solid line). 31

Figure 18. The maximum temperature at extinction for counterflow methane flames is plotted as a function of the percentage of a thermal agent added to air divided by the amount calculated to be required for flame extinguishment. 31

Figure 19. Maximum calculated flame temperatures are plotted against methane and oxidizer flow exit velocity magnitudes for a series of methane/air opposed flow diffusion flames diluted with a surrogate agent similar to argon, but with $C_p = 0$. Symbols correspond to the percentage of surrogate agent added. 33

Figure 20. Values of maximum flame temperature at extinction are plotted as a function of fuel and oxidizer extinction velocity magnitudes for a range of concentrations of argon and a similar surrogate agent having $C_p = 0$. The solid line is the result of the regression fits shown in Figure 17..... 33

Figure 21. Temperature is plotted as a function of distance from the fuel exit for methane flames burning in air and air mixed with 60% of a diluent having similar properties to Ar, but with zero heat capacity. Fuel and air exit velocity magnitudes are 25 cm/s for both flames..... 34

Figure 22. Calculated methane and oxygen mole fractions are shown on a semi-log plot as a function of distance from the fuel exit for methane flames burning in air (open symbols) and air mixed with 60% of a diluent having similar properties to Ar, but with zero heat capacity. Fuel and air exit velocity magnitudes are 25 cm/s for both flames. 34

Figure 23. Calculated flame temperature is plotted as a function of distance from the fuel exit for methane/air diffusion flames where the oxidizer is diluted with 5% of either argon or the hypothetical agent X which reacts to form Y with $E_a = 25.1$ kJ/mole and $\Delta H_{X\text{-}Y} = 96.1$ kJ/mole. Methane and oxidizer exit velocity magnitudes are 25 cm/s. 36

Figure 24. The mole fractions of X and Y are plotted as a function of distance from the fuel exit for a methane flame burning in air with 5% added X. X reacts to form Y with $E_a = 25.1$ kJ/mole and

ΔH_{X-Y} = 96.1 kJ/mole. The spatial variation of temperature is also shown as the solid line. Methane and oxidizer exit velocity magnitudes are 25 cm/s. 36

Figure 25. The mole fractions of X and Y are plotted as a function of distance from the fuel exit for a methane flame burning in air with 5% added X. X reacts to form Y with E_a = 58.6 kJ/mole and ΔH_{X-Y} = 96.1 kJ/mole. The spatial variation of temperature is also shown as the solid line. Methane and oxidizer exit velocity magnitudes are 25 cm/s. 38

Figure 26. The mole fractions of X and Y are plotted as a function of distance from the fuel exit for a methane flame burning in air with 5% added X. X reacts to form Y with E_a = 83.7 kJ/mole and ΔH_{X-Y} = 96.1 kJ/mole. The spatial variation of temperature is also shown as the solid line. Methane and oxidizer exit velocity magnitudes are 25 cm/s. 38

Figure 27. Values of maximum flame temperature for methane flames burning in air diluted with 5% X are plotted as a function of the energy of activation for the conversion of X to Y. Methane and oxidizer exit velocity magnitudes are 25 cm/s. 39

Figure 28. Maximum calculated flame temperatures are plotted against methane and oxidizer exit velocity magnitudes for a series of methane/air opposed flow diffusion flames diluted with agent X which reacts to form Y with E_a = 41.8 kJ/mole and ΔH_{X-Y} = 96.1 kJ/mole. Symbols correspond to the percentage of added X. 39

Figure 29. Maximum calculated flame temperatures are plotted against methane and oxidizer exit flow velocity magnitudes for a series of methane/air opposed flow diffusion flames diluted with argon and agent X (E_a = 41.8 kJ/mole and ΔH_{X-Y} = 96.1 kJ/mole). 40

Figure 30. Maximum calculated flame temperatures are plotted against methane and oxidizer exit flow velocity magnitudes for a series of methane/air opposed flow diffusion flames diluted with agent X which reacts to form Y with E_a = 41.8 kJ/mole and ΔH_{X-Y} = 192.1 kJ/mole. Symbols correspond to the percentage of added X. 40

Figure 31. Values of maximum flame temperature at extinction are plotted as a function of fuel and oxidizer exit velocity magnitudes for air diluted with a range of concentrations of argon and surrogate agent X having ΔH_{X-Y} = 96.1 kJ/mole or 192.1 kJ/mole. The solid line is the result of the regression fits shown in Figure 17. 41

Figure 32. Maximum calculated flame temperatures are plotted against methane and oxidizer exit velocity magnitudes for a series of methane/air opposed flow diffusion flames diluted with $C_4F_9OCH_3$. Symbols correspond to the percentage of added $C_4F_9OCH_3$. 42

Figure 33. Droplet evaporation time as a function of initial droplet diameter. 48

Figure 34. An illustration of a typical boiling curve associated with quenching of a hot surface. 49

Figure 35. Calculated boiling curve in the convective regime. 51

Figure 36. Calculated boiling curve in the transition and film boiling regimes. 53

EXECUTIVE SUMMARY

The use of halons for fire fighting is being phased out due to their deleterious effects on stratospheric ozone. This report summarizes the first-year findings of a three-year study designed to characterize and identify super-effective thermal fire-fighting agents as possible replacements for these widely used compounds. Three distinct aspects related to the effectiveness of potential thermal agents have been considered. First, existing thermodynamic databases maintained by NIST have been searched in order to identify chemical compounds which are predicted to extract large amounts of heat from a combustion zone. Second, detailed chemical kinetic modeling has been used to characterize the effects of thermal agents on an idealized flame system, namely, a methane/air counterflow diffusion flame. Third, empirical heat transfer correlations for spray cooling of a surface have been used to estimate the efficiencies of surface cooling by thermal agents.

The database search used two primary sources—the Design Institute for Physical Properties database containing 1458 compounds from 83 family types and a smaller database, REFPROP, containing 43 compounds which is tailored to refrigerant applications. Additional substances were included which are not well represented in these databases. Compounds having 1) high heats of vaporization, 2) liquid-phase heat capacities, and 3) total heat absorption due to phase changes (if applicable), heating of a liquid (if applicable), and the heating of the gas phase to combustion temperatures were identified. The results are reported in tables of compounds ordered in terms of their ability to extract heat.

Detailed chemical kinetic modeling of opposed flow methane diffusion flames burning in air and air diluted with thermal agents has been used to obtain insights into the effectiveness of thermal agents and their mechanisms of flame extinction. Values of fuel and air velocities which induce flame extinction were determined as a function of agent concentration. Comparison of the calculated results for burning in two types of oxidizer, air diluted with added nitrogen and a synthetic "air" having nitrogen replaced by argon and diluted with additional argon, with corresponding experimental measurements of the concentrations necessary to extinguish a counterflow diffusion flame showed that extinguishment occurs when the maximum calculated flame temperature drops to approximately 1550 K for fuel and oxidizer velocities of a few tens of cm/s. Using this result, extinguishing calculations were then estimated for carbon dioxide, argon, helium, and water. Published experimental extinguishment concentrations for these thermal agents are unavailable for methane flames, but a strong correlation was found with agent extinguishing concentrations determined in cup burner tests using liquid heptane as fuel. A series of calculations were performed for one of compounds identified as likely to be particularly effective at extracting heat during the database search, methoxy-nonafluorobutane. An extinguishing concentration of 5.5% was predicted, which is close to unpublished experimental cup burner values of 6.1%

An advantage of detailed kinetic modeling studies is that surrogate agents having properties which are not physically realizable can be used to investigate specific details concerning extinguishment. A surrogate agent was specified which reacted over different temperature ranges to extract a predetermined amount of heat. The calculations showed that the effectiveness of this agent was independent of the location of heat extraction relative to the flame zone. In a second series of calculations a surrogate agent was used to isolate the role of dilution on extinguishment. When the agent, which was incapable of extracting heat, was added to the air, much higher concentrations were required to extinguish the flame than when heat was extracted. Details of the calculations revealed that extinguishment ultimately occurred due to oxygen passing through the flame zone.

Calculations of droplet evaporation times using the classical d^2-law for the five fluids (water, lactic acid, $C_3F_5H_3O$, HFE7100, and R338mccq) identified as having the highest latent heat of vaporization (per unit mass) by the database searches were performed as part of the surface cooling studies. Empirical heat transfer

correlations from the spray surface quenching literature were used to assess the surface cooling characteristics of these fluids for various heat transfer regimes. Based on these calculations, water and lactic acid appear to be more effective than the other three fluids for surface cooling applications.

Recommendations are included for additional studies during the second year of the project.

I. INTRODUCTION

The use of halons for fire fighting is being phased out due to their deleterious effects on stratospheric ozone. This report summarizes the first-year findings of a three-year study designed to characterize and identify super-effective thermal fire-fighting agents as possible replacements for these effective compounds. "Thermal" agents refer to compounds which act simply by extracting heat from a flame zone and lowering the temperature to a point where combustion can no longer be sustained. These types of agents should be contrasted with "chemical" agents which generate active chemical species (e.g., the bromine atoms generated by halons) which interfere with the radical chain branching mechanisms required to sustain combustion.

There are a number of endothermic physical processes which can extract heat from a gaseous flame zone, thus lowering the temperature and ultimately leading to flame extinguishment. These include simple heating (i.e., heat capacity) of an agent, phase changes such as vaporization of a liquid or sublimation of a solid, endothermic molecular decomposition (note that this process is classed as a physical process as long as the initial agent and its products do not participate in the combustion chemistry), and simple dilution which can modify flame temperatures by spreading the heat release over larger volumes and by slowing three-body reactions by lowering species collision rates. The flame temperature is also expected to be a function of the thermal diffusivity of an agent.

Another potentially effective way for thermal agents to extinguish a flame fueled by liquids or solids is to interact with the fuel surface to lower the temperature to a point where the fuel generation rate is insufficient to maintain combustion. This mechanism for fire extinguishment has not been extensively studied, and the physical properties which determine the effectiveness of an agent operating in this mode are not known.

During the first year of the investigation three distinct aspects related to the effectiveness of potential thermal agents have been considered. First, existing thermodynamic data bases maintained by NIST have been searched in order to identify chemical compounds which are predicted to extract large amounts of heat as the temperature is raised. Second, detailed chemical kinetic modeling has been used to characterize the effects of thermal agents on an idealized flame system, namely, a methane/air counterflow diffusion flame. Third, empirical heat transfer correlations for spray cooling of a surface have been used to estimate the efficiencies of surface cooling by thermal agents which are expected to be very efficient at extracting heat from combustion regions.

The following three sections summarize the findings of each of these approaches. The results are then used as the basis for recommending that the investigation be carried into a second year in order to further validate the current findings and to provide initial laboratory testing of several potentially effective thermal agents.

II. SCREENING OF THERMOPHYSICAL PROPERTIES DATABASES FOR SUPER EFFECTIVE THERMAL AGENTS

The objective of this sub-task was to search thermophysical property databases and identify substances that may be suitable candidates for fire extinguishing agents based on their thermophysical properties. We identified two thermophysical property databases to search. The first was the DIPPR (Design Institute for Physical Properties) Database, version 9.02 [1] which contained 1458 substances from 83 family types. The families are listed in Table 1. The second database, REFPROP, Version 5, [2] is a much smaller database

Table 1. Family Types in the DIPPR Database

1 n-Alkanes	29 Cycloaliphatic alcohols	57 Other amines, imines
2 Methylalkanes	30 Aromatic alcohols	58 Nitriles
3 Dimethylalkanes	31 Polyols	59 C,H,NO2 compounds
4 Other alkanes	32 n-aliphatic acids	60 Isocyanates/Diisocyana
5 Cycloalkanes	33 Other aliphat acids	61 Mercaptans
6 Alkylcyclopentanes	34 Dicarboxylic acids	62 Sulfides/Theophenes
7 Alkylcyclohexanes	35 Aromatic carbox. acids	63 Polyfunctional acids
8 Multi-ring cycloalkanes	36 Anhydrides	64 Polyfunctional esters
9 1-alkynes	37 Formates	65 Oth. Polyfunctional C,
10 2,3,4-alkenes	38 Acetates	66 Polyfunctional nitrile
11 Methylalkenes	39 Propionates & Butyrates	67 Nitroamines
12 Ethyl & higher alkenes	40 Other sat. aliph esters	68 Polyfunc. Amides/Amine
13 Cycloalkenes	41 Unsat. aliphatic esters	69 Polyfunctional C,H,O,N
14 Dialkenes	42 Aromatic esters	70 Polyfunctional C,H,O,S
15 Alkynes	43 Aliphatic ethers	71 Polyfunctional C,H,O,h
16 n-alkylbenzenes	44 Other Ethers/Diethers	72 Polyfunc C,H,N,halide
17 Other alkylbenzenes	45 Epoxides	73 Other Polyfunc. Organi
18 Other monoaromatics	46 Peroxides	74 Elements
19 Napthalenes	47 C1/C2 Aliphatic chlorid	75 Silanes/Siloxanes
20 Other condensed rings	48 C3 & higher aliph. chlo	76 Organic-Inorganic
21 Diphenyl/Polyaromatics	49 Aromatic chlorides	77 Inorganic acids
22 Terpenes	50 C,H,Br compounds	78 Inorganic bases
23 Other hydrocarbon rings	51 C,H,I compounds	79 Organic salts
24 Inorganic gases	52 C,H,F compounds	80 Sodium salts
25 Aldehydes	53 C,H multihalog cmps	81 Other inorganic salts
26 Ketones	54 n-Aliphatic prim. amine	82 Inorganic halides
27 n-alcohols	55 Other aliphatic amines	83 Other inorganics
28 Other alcohols(aliph.)	56 Aromatic amines	

tailored to alternative refrigerants. It contains 43 refrigerants including many candidates for replacing HCFCs. Some are fluorinated ethers (E134, E245) that are not present in the DIPPR database.

In addition, we wanted to include representative substances from some families of chemicals not well represented in existing thermophysical property databases, such as fluorinated ethers, alcohols and amines. The fluorinated ethers are especially interesting since their atmospheric lifetimes may be significantly lower than those of chlorofluorocarbons. [3] Some of these have been identified as possible replacements for blowing agents, refrigerants, fire suppression agents, and as solvents. [4,5,6,7,8,9] We selected several cyclic fluorinated ether compounds (fluorinated oxiranes, oxetanes and furans), some non-cyclic methyl ethers (HFE116, HFE125), fluorinated methyl ethyl ethers with two or fewer hydrogen atoms (HFE 227me, HFE236me), and some larger fluorinated ethers--perfluorodimethoxymethane ($CF_3OCF_2OCF_3$), perfluoropropyltrifluoromethyl ether ($CF_3OCF_2CF_2CF_3$), heptafluoropropyl-1,2,2,2-tetrafluoroethyl ether ($CF_3CHFOCF_2CF_2CF_3$) and methoxy-nonafluorobutane ($C_4F_9OCH_3$, HFE7100). In addition to the fluorinated ethers, we added two fluorinated amines to the list of substances to search and also the alternative refrigerant HFC-338mccq ($CH_2FCF_2CF_2CF_3$) and the fluorinated alcohol 2,2,3,3,3-pentafluoropropanol ($CF_3CF_2CH_2OH$).

The physical properties that are important for thermal agents are high latent heats of vaporization and high liquid and vapor heat capacities. We first searched the databases and the additional fluids mentioned above for high latent heats of vaporization. For fluids where data were unavailable, we estimated the critical properties using the NIST Structures and Properties program [10] and then estimated the latent heats using the approach of Fishtine [11]. We then eliminated substances on the list that either were identified as flammable, toxic, or

had known ozone depletion problems. However, we did not have complete information on toxicity so some substances that appear on our final list will need to be investigated further to determine if there are potential deleterious health effects. We also did not use global warming potential or electrical conductivity as screening parameters. If one considers global warming potential, then the fully fluorinated (perfluorinated) alkanes such as R218 and decafluorobutane would probably have to be ruled out. We used information in the DIPPR database on flash points and upper and lower flammability limits. The DIPPR database does not contain any information on toxicity or other health effects. For this information we used manufacturers safety data sheets and Hawley [12]. We also used the web site at http://chemfinder.camsoft.com/ that gives information on ozone depletion and global warming.

Table 2 gives the list of compounds that remained, in order of decreasing heat of vaporization at the normal boiling point and includes R13B1 and water for reference. Table 3 identifies the source of the property data for critical points, normal boiling points, latent heat of vaporization, and liquid heat capacity. The general trend shown in Table 2 is quite predictable--the larger molecules have higher boiling points and higher heats of vaporization. Lactic acid is the only unusual fluid that appears is Table 2--all other fluids are basically {C, F, H}, {C, F} or {C, F, O} compounds. Lactic acid, CH3CH(OH)COOH, is a strong irritant to the skin and corrosive in concentrated form and would not be a suitable agent. However, it may be at least partially soluble in fluorinated ethers such as HFE134 or in alternative refrigerants such as R227ea. It would be interesting to test a mixture of lactic acid with some of the other fluids on the list to see if a small amount of dissolved lactic acid would enhance the latent heat of vaporization.

The second property we searched on was liquid heat capacity at the normal boiling point. When data were unavailable, the liquid heat capacity was estimated using the Chueh-Swanson method. [13] This method provides the liquid heat capacity at 20 °C based on the structure of a compound. The results are shown in Table 4 in order of decreasing liquid-phase heat capacity at the normal boiling point and include R13B1 and water for reference. Again, any compounds that were known to be flammable or toxic or to have known ozone depletion problems were eliminated. Table 4 indicates the same trend that was seen in Table 2, i.e., that larger compounds have higher boiling points and higher heats of vaporization and heat capacities. Also, in general, the ethers have higher boiling points and higher heats of vaporization at their normal boiling points than their alkane analogs. The fluorinated alcohol has a high boiling point due to the hydrogen bonding that occurs in alcohols.

In addition to looking at the latent heat of vaporization and the liquid heat capacity at the normal boiling point, one may also look at the total heat involved in going from the fluid at room temperature up to a temperature of 1400 K, which was selected as a representative combustion temperature. Other choices are possible including the value of 1550 K identified later by the detailed chemical kinetic modeling. The actual value used is unlikely to affect the relative ordering of agents. The total heat absorbed consists of three contributions,

$$\Delta H^{Total} = \Delta H_1 + \Delta H_2 + \Delta H_3 \quad , \qquad (1)$$

where the first contribtion, ΔH_1, is the heat involved in taking the liquid from room temperature up to the normal boiling point,

$$\Delta H_1 = \int_{298\,K}^{T_b} C_p^{liquid}\, dT \, . \qquad (2)$$

Since the heat capacity of a liquid does not change significantly over a small temperature range, we used the value of liquid heat capacity at the normal boiling point. If this was unavailable, we estimated the liquid phase

Table 2. Results of Search for Compounds with High Heat of Vaporization at the Normal Boiling Point

Compound	T_b(K)	ΔH_{vap} (kJ/mol)
lactic acid, $C_3H_6O_3$	455	59.2
water	373.1	40.0
2,2,3,3,3-pentafluoropropanol, $C_3F_5H_3O$	353.15	37.6
perfluoro-2-butyltetrahydrofuran, $C_8F_{16}O$	375.15	35.4
methoxy-nonafluorobutane, HFE7100	334.0	30.3
heptafluoropropyl-1,2,2,2-tetrafluoroethyl ether	315.2	29.0
difluoromethyl-1,2,2,2-tetrafluoroethyl ether, E236me	296.5	26.9
1,1,1,2,2,3,3,4-octafluorobutane, R338mccq	301	26.8
tris(difluoromethyl)amine, $C_3H_3F_6N$	275	25.8
1,1,2,2-tetrafluorodimethylether, E134	279.4	25.4
1,1,1,2,3,3-hexafluoropropane, R236ea	279.7	25.1
perfluorotrimethylamine, C_3F_9N	264	23.9
trifluoromethyl-1,2,2,2-tetrafluoroethyl ether, E227me	263.6	23.7
octafluorocyclobutane, C_4F_8	267	23.2
decafluorobutane, C_4F_{10}	271	23.2
perfluorodimethoxymethane, $CF_3OCF_2OCF_3$	263	23.1
perfluoropropylmethyl ether, $C_3F_7OCF_3$	279.9	22.8
bis(trifluoromethyl)ether, E116	257	22.8
octafluorofuran, C_4F_8O	272.42	22.7
1,1,2,2-tetrafluoroethane, R134	250	22.5
1,1,1,2-tetrafluoroethane, R134a	247	22.3
perfluoroisobutane, C_4F_{10}	252.45	22.0
octafluoro-2-butene	270.4	21.7
1,1,1,2,3,3,3-heptafluoropropane, R227ea	257.5	21.4
perfluorooxetane, C_3F_6O	244.0	20.9
pentafluorodimethylether, E125	235	20.0
octafluoropropane, R218	236.4	19.7
hexafluoropropylene	243.5	19.4
pentafluoroethane, R125	225.2	19.1
bromotrifluoromethane, R13B1	215.26	17.4
hexafluoroethane, R116	194.95	16.1

heat capacity at 20 °C using the method of Chueh and Swanson. [13] The second term, ΔH_2, is the latent heat of vaporization at the normal boiling point. The third contribution, ΔH_3, is found by integrating the gas-phase heat capacity from the normal boiling point to 1400 K,

$$\Delta H_3 = \int_{T_b}^{1400\,K} C_p^{gas}\, dT\,. \qquad (3)$$

We estimated the gas phase heat capacities using the method of Rihani and Doraiswamy [14], which is based on structural contributions. For agents with boiling points below 298 K, the total heat involved is just the contribution ΔH_3. Table 5 summarizes the results of this computation, with compounds listed in order of their ΔH^{total} expressed on a molar basis (kJ/mol). Table 6 gives the same quantity, but expressed on a mass basis

Table 3. References for Property Data (Critical Point, Normal Boiling Point, Heat of Vaporization, Liquid Heat Capacity)

Compound	References
perfluoro-2-butyltetrahydrofuran, $C_8F_{16}O$	15, 13, 11
methoxy-nonafluorobutane, HFE7100	16, 13, 11
lactic acid, $C_3H_6O_3$	1
heptafluoropropyl-1,2,2,2-tetrafluoroethyl ether	10, 13, 11
decafluorobutane, C_4F_{10}	1
perfluoropropylmethyl ether, $C_3F_7OCF_3$	17, 13, 11
perfluorodimethoxymethane, $CF_3OCF_2OCF_3$	18, 13, 11
octafluoro-2-butene	1
octafluorofuran, C_4F_8O	17, 13, 11
octafluorocyclobutane, C_4F_8	1
perfluorotrimethylamine, C_3F_9N	10, 13, 11
1,1,1,2,3,3,3-heptafluoropropane, R227ea	2
perfluoroisobutane, C_4F_{10}	4, 13, 11
tris(difluoromethyl)amine, $C_3H_3F_6N$	10, 13, 11
trifluoromethyl-1,2,2,2-tetrafluoroethyl ether, E227me	19, 13, 11
1,1,1,2,2,3,3,4-octafluorobutane, R338mccq	20, 13, 11
1,1,1,2,3,3-hexafluoropropane, R236ea	2
difluoromethyl-1,2,2,2-tetrafluoroethyl ether, E236me	19, 13, 11
octafluoropropane, R218	2
2,2,3,3,3-pentafluoropropanol, $C_3F_5H_3O$	21, 13, 11
perfluorooxetane, C_3F_6O	18, 13, 11
1,1,2,2-tetrafluorodimethylether, E134	22
bis(trifluoromethyl)ether, E116	10, 13, 11
hexafluoropropylene	1
pentafluorodimethylether, E125	17, 13, 11
pentafluoroethane, R125	2
1,1,2,2-tetrafluoroethane, R134	2
hexafluoroethane, R116	2
1,1,1,2-tetrafluoroethane, R134a	2
bromotrifluoromethane, R13B1	1
water	1

(kJ/kg). We have also included some common agents such as nitrogen, argon, water and carbon dioxide for comparison.

The results of Table 5 indicate that the top candidates for streaming agents (defined here as having boiling points higher than 293 K), on a molar basis, are perfluoro-2-butyltetrahydrofuran, methoxy-nonafluorobutane, heptafluoropropyl-1,2,2,2-tetrafluoroethyl ether, and 1,1,1,2,2,3,3,4-octafluorobutane. Table 6 indicates that methoxy-nonafluorobutane (HFE7100) is high on the list when expressed on a mass basis. Methoxy-nonafluorobutane is available commercially [16], the others are not available commercially but have been synthesized and used for research [17,18,19]. The top total-flooding candidates (defined as having boiling points lower than 293 k) are perfluoropropyltrifluromethyl ether, perfluoroisobutane, decafluorobutane, and

Table 4. Results of Search for Compounds with High Liquid Phase Heat Capacities at the Normal Boiling Point

Compound	T_b (K)	C_p (J/mol K)
perfluoro-2-butyltetrahydrofuran, $C_8F_{16}O$	375.15	364.2
methoxy-nonafluorobutane, HFE7100	334.0	292.8
lactic acid, $C_3H_6O_3$	455	290.1
heptafluoropropyl-1,2,2,2-tetrafluoroethyl ether	315.2	269.6
decafluorobutane, C_4F_{10}	271	241.4
perfluoropropylmethyl ether, $C_3F_7OCF_3$	279.9	231.9
perfluorodimethoxymethane, $CF_3OCF_2OCF_3$	263	226.0
octafluoro-2-butene	270	218.1
octafluorofuran, C_4F_8O	272.42	217.6
octafluorocyclobutane, C_4F_8	267	208.1
perfluorotrimethylamine, C_3F_9N	264	204.0
1,1,1,2,3,3,3-heptafluoropropane, R227ea	257.5	200.1
perfluoroisobutane, C_4F_{10}	252.45	196.8
tris(difluoromethyl)amine, $C_3H_3F_6N$	275	194.6
trifluoromethyl-1,2,2,2-tetrafluoroethyl ether, E227me	263.6	187.9
1,1,1,2,2,3,3,4-octafluorobutane, R338mccq	301	186.4
1,1,1,2,3,3-hexafluoropropane, R236ea	279.7	185.4
difluoromethyl-1,2,2,2-tetrafluoroethyl ether, E236me	296.5	184.9
octafluoropropane, R218	236.4	183.8
2,2,3,3,3-pentafluoropropanol, $C_3F_5H_3O$	353.15	173.5
perfluorooxetane, C_3F_6O	244.0	171.9
1,1,2,2-tetrafluorodimethylether, E134	279.4	150.8
bis(trifluoromethyl)ether, E116	257	150.3
hexafluoropropylene	243.5	148.2
pentafluorodimethylether, E125	235	147.1
pentafluoroethane, R125	225.2	134.2
1,1,2,2-tetrafluoroethane, R134	250	133.3
hexafluoroethane, R116	194.95	130.6
1,1,1,2-tetrafluoroethane, R134a	247	129.4
bromotrifluoromethane, R13B1	215.26	100.3
water	373.1	76.0

octafluorocyclobutane. Of these, decafluorobutane and octafluorocyclobutane are available commercially. [23] All of these compounds contain only C, H, F and O. If any of these fluids show promise as fire extinguishing agents, mixtures may be investigated in order to adjust the boiling points and possibly to enhance effectiveness beyond that expected for simple linear mixing of the components.

III. DETAILED CHEMICAL KINETIC MODELING OF EXTINGUISHMENT BEHAVIOR FOR THERMAL AGENTS IN METHANE/AIR DIFFUSION FLAMES

A. Introduction

Combustion is a complicated physical process involving the interaction of fluid flow and chemical reaction accompanied by heat release. It is now recognized that combustion involves a large number of chemical

Table 5. Results of Search for Compounds with High ΔH^{Total} (Molar Basis)

Compound	T_b(K)	ΔH^{Total} (kJ/mol)
perfluoro-2-butyltetrahydrofuran, $C_8F_{16}O$	375.2	608.4
heptafluoropropyl-1,2,2,2-tetrafluoroethyl ether	315.2	421.9
methoxy-nonafluorobutane, HFE7100	334	407.6
perfluoropropyltrifluoromethyl ether,$CF_3OCF_2CF_2CF_3$	279.9	336.3
perfluoroisobutane, C_4F_{10}	252.5	321.2
1,1,1,2,2,3,3,4-octafluorobutane, R338mccq	301	321.0
decafluorobutane, C_4F_{10}	271	318.5
octafluorocyclobutane, C_4F_8	267	303.2
perfluorotrimethylamine, C_3F_9N	264	293.8
lactic acid, $C_3H_6O_3$	455	292.9
perfluorodimethoxymethane, $CF_3OCF_2OCF_3$	263	286.8
octafluorofuran, C_4F_8O	272.4	289.8
2,2,3,3,3-pentafluoropropanol, $C_3F_5H_3O$	353.15	280.8
octafluoro-2-butene	270	261.9
tris(difluoromethyl)amine, $C_3H_3F_6N$	275	256.5
trifluoromethyl-1,2,2,2-tetrafluoroethyl ether, E227me	263.6	255.3
perfluorooxetane, C_3F_6O	244.0	252.9
octafluoropropane, R218	236.4	250.8
difluoromethyl-1,2,2,2-tetrafluoroethyl ether, E236me	296.5	239.4
1,1,1,2,3,3,3-heptafluoropropane, R227ea	257.5	236.5
1,1,1,2,3,3-hexafluoropropane, R236ea	279.7	222.2
bis(trifluoromethyl)ether, E116	257	196.2
hexafluoropropylene	243.5	192.9
pentafluorodimethylether, E125	235	183.8
hexafluoroethane, R116	194.95	181.1
1,1,2,2-tetrafluorodimethylether, E134	279.4	170.2
pentafluoroethane, R125	225.2	166.8
1,1,1,2-tetrafluoroethane, R134a	247	156.8
1,1,2,2-tetrafluoroethane, R134	250	152.8
bromotrifluoromethane, R13B1	215.26	110.9
water	373.1	87.5
carbon dioxide	n/a	56.2
nitrogen	77.4	34.7
argon	87.3	22.9

species and reactions. The most important reactions are those involving radical species such as OH, HO_2, and O and H atoms. The most dominant reaction is usually recognized as the chain branching reaction leading to the breaking of the oxygen bond, i.e.,

$$H + O_2 \rightarrow OH + O \quad . \qquad (4)$$

Table 6. Results of Search for Compounds with High ΔH^{Total} (Mass Basis)

Compound	T_b(K)	ΔH^{total} (kJ/kg)
water	373.1	4855.7
lactic acid, $C_3H_6O_3$	455	3251.6
2,2,3,3,3-pentafluoropropanol, $C_3F_5H_3O$	353.15	1872.0
methoxy-nonafluorobutane, HFE7100	334	1630.4
1,1,1,2,2,3,3,4-octafluorobutane, R338mccq	301	1588.7
1,1,1,2-tetrafluoroethane, R134a	247	1536.8
tris(difluoromethyl)amine, $C_3H_3F_6N$	275	1535.5
perfluorooxetane, C_3F_6O	244.0	1523.2
octafluorocyclobutane, C_4F_8	267	1515.8
1,1,2,2-tetrafluoroethane, R134	250	1497.6
heptafluoropropyl-1,2,2,2-tetrafluoroethyl ether	315.2	1475.0
perfluoro-2-butyltetrahydrofuran, $C_8F_{16}O$	375.2	1462.3
1,1,1,2,3,3-hexafluoropropane, R236ea	279.7	1461.4
1,1,2,2-tetrafluorodimethylether, E134	279.4	1442.0
difluoromethyl-1,2,2,2-tetrafluoroethyl ether, E236me	296.5	1424.7
1,1,1,2,3,3,3-heptafluoropropane, R227ea	257.5	1390.9
pentafluoroethane, R125	225.2	1389.8
trifluoromethyl-1,2,2,2-tetrafluoroethyl ether, E227me	263.6	1372.4
pentafluorodimethylether, E125	235	1351.3
perfluoroisobutane, C_4F_{10}	252.5	1349.6
octafluorofuran, C_4F_8O	272.4	1341.5
decafluorobutane, C_4F_{10}	271	1338.2
octafluoropropane, R218	236.4	1333.8
perfluorotrimethylamine, C_3F_9N	264	1329.3
perfluoropropyltrifluoromethyl ether, $CF_3OCF_2CF_2CF_3$	279.9	1323.9
hexafluoroethane, R116	194.95	1312.2
octafluoro-2-butene	270	1309.2
perfluorodimethoxymethane, $CF_3OCF_2OCF_3$	263	1303.5
hexafluoropropylene	243.5	1285.8
carbon dioxide, CO_2	n/a	1276
bis(trifluoromethyl)ether, E116	257	1273.9
nitrogen, N_2	77.4	1238.3
bromotrifluoromethane, R13B1	215.26	744.7
argon	87.3	573.2

Subsequent reactions involving these free radicals release heat and ultimately maintain the combustion. Reaction (4) is strongly temperature dependent, and extinguishment of a flame is expected to occur when the temperature is lowered to a point where the rate of generation of free radicals becomes so slow that the overall reactions cannot generate sufficient heat release to overcome the heat losses from the reaction zone (primarily by thermal diffusion, radiation, and incomplete combustion).

During the past two decades the understanding of the chemical kinetics involved in combustion has reached the point where realistic detailed mechanisms including large numbers of reactants and reactions can be written for simple combustion systems, and mathematical techniques have been developed for simultaneously solving the large number of differential equations which result. While still involving significant approximations (some of which are discussed below), such modeling has developed to the point where it can be used to gain useful insights into the behavior of practically relevant flames.

A number of different types of combustion systems have been modeled including plug flow reactors, perfectly stirred reactors, premixed flames, and opposed flow laminar diffusion flames. For studies of fire extinguishment, we have chosen to use an opposed flow laminar diffusion flame model because, for the vast majority of fires, the fuel and air are initially separated and therefore burn as diffusion flames. Most fires are large enough to be turbulent, so a laminar flame model is not strictly correct. However, the most widely used model for turbulent combustion incorporating detailed chemistry is the laminar flamelet concept which models the combustion as laminar flame sheets which are subject to the local strain rate field associated with the motions of the fluid induced by the fire. [24,25] Thus, the opposed flow diffusion flame should be the most appropriate detailed chemical kinetic model available for describing fire behavior.

There are three configurations of opposed flow diffusion flames which have been described in the literature—opposed jet, flow over a porous cylinder, and flow over a porous sphere. For the porous bodies, fuel typically flows from the surface, and the surrounding flow is the oxidizer. The three configurations are related in that a diffusion flame is stabilized in the region near the stagnation point in the flow. Numerous papers in the literature discuss these types of flames. Two excellent reviews have been provided by Tsuji [26] and Dixon-Lewis [27]. The review by Tsuji includes a discussion of the use of such burners to experimentally characterize flame inhibition. Examples of early studies include References [28], [29], [30], [31], and [32]. All three configurations are represented. Recently, an opposed jet experiment has been used to investigate potential replacement agents for halons. [33]

The most common of the three configurations used in the recent past is the opposed jet laminar diffusion flame. This configuration has also been the choice for most of the available modeling investigations of opposed flow flames. For these reasons, we have chosen this configuration for this investigation.

The review of Dixon-Lewis focuses on detailed chemical kinetic modeling of opposed flow diffusion flames. [27] Detailed chemical models were initially developed in a series of steps. The earliest were designed to describe reactions between H_2 and O_2. The next step was to include CO with the H_2 and O_2. After these mechanisms were sufficiently developed, they were used as the basis for extended mechanisms describing the oxidation of methane. By the early 1980s researchers had begun to calculate the structure of opposed flow laminar methane/air diffusion flames. The earliest such calculation we have identified is that of Hahn and Wendt [34] which was published in 1981. This was followed by the work of Dixon-Lewis et al. [35], Smooke et al. [36], Dixon-Lewis et al. [37], Puri et al. [38], and Chelliah et al. [39].

Before discussing the findings of these studies, it is important to introduce and clarify some ideas concerning the parameters used to characterize the flow field and its potential interactions with combustion reactions. Much of what follows is based on a review paper by Law. [40]

The degree of interaction between combustion and a flow field is often treated using the concept of flame stretch. This is particularly true for laminar premixed flames. Flame stretch, K, is defined as

$$K = \frac{1}{A}\frac{dA}{dt}, \qquad (5)$$

where A is the infinitesimal area of an arbitrary flame surface lying within the flame structure, e.g., an isotherm or isopleth, and t represents time. In the general case, flame stretch can be broken into three individual contributions due to aerodynamic strain, flame curvature, and flame motion. For a planar, axisymmetric diffusion flame, however, the latter two effects are absent and K is simply equal to the strain rate within the planar surface, b, with

$$b = \frac{\partial v}{\partial r}, \qquad (6)$$

where cylindrical coordinates have been introduced with z and r the directions perpendicular and parallel to the flame sheet, respectively, and u and v are the velocities in these directions. For the planar flame u is assumed to be only a function of z. The velocities u and v are dependent on each other through the continuity equation, which for a cylindrical coordinate system is written as

$$\frac{\partial(r\rho u)}{\partial z} + \frac{\partial(r\rho v)}{\partial r} = 0, \qquad (7)$$

with ρ equal to the local density.

Law discusses the effects of flame stretch on flame behavior in terms of the different roles of velocity gradient elements tangent to and normal to the flame surface. He notes that there has been a great deal of confusion in the literature in distinguishing between the roles of each element. He argues that it is the normal element of the axial velocity gradient which determines the residence time within the flame and that the Damkohler number, *Da*, defined as the ratio of the characteristic flow time to a characteristic reaction time, should be based on this velocity gradient element. As we shall see shortly, *Da* is a dominant parameter for describing flame extinction. For now, it is important to note that for planar diffusion flames the most important characteristic flow parameter is the element of the axial velocity gradient in the axial direction,

$$a = \frac{\partial u}{\partial z}. \qquad (8)$$

Returning now to the discussion of early detailed kinetic investigations of methane/air diffusion flames, the paper by Dixon-Lewis et al. is particularly interesting because it involved an intercomparison of calculated results for an opposed flow methane/air diffusion flame by five different research groups. [35] Calculated flame structures were compared with the experimental measurements of Tsuji and Yamaoka [41,42] for the configuration of flow over a porous cylinder. All of the researchers used the same model for the velocity field. A similarity transform was used to convert the two-dimensional flow field to a pseudo one-dimensional flow, thus greatly reducing the amount of computation required. The coordinate system employed for these calculations was actually rectilinear, but the following discussion will be in terms of cylindrical coordinates. The opposed flows for ambient locations outside of the reacting boundary layer were assumed to be potential flows generated from point sources located at infinity. One appealing aspect of such a flow is that the characteristic strain rate, usually defined as the radial velocity gradient element in the radial direction,

$$b_p = \frac{\partial v}{\partial r} \quad , \qquad (9)$$

is constant in the isothermal region. The continuity equation allows the following relationship between a_p and b_p to be derived,

$$a_p = \frac{\partial u}{\partial z} = -\frac{1}{2} b_p . \qquad (10)$$

Dixon et al. concluded that the models described the qualitative flame structure quite well, but that the quantitative agreement was not perfect. [35] In particular, they argued that the assumption of potential flow was inadequate to describe the actual flow field. The results from the different investigators within the intercomparison also differed somewhat, and additional study was suggested to identify the sources of these variations.

While the strain rate dictated by the potential flow provided a natural variable to characterize the velocity field, the authors also noted that the scalar dissipation rate at the stoichiometric surface of the flame, χ_s, is more commonly used to describe the effect of strain on diffusion flames in turbulent models. [24,25] The scalar dissipation rate is defined as

$$\chi = 2D\left(\frac{\partial Z}{\partial x}\right)^2 \quad , \qquad (11)$$

where D is a molecular diffusion coefficient and Z is the fuel mixture fraction, a conserved scalar. An expression was provided which allowed χ_s to be calculated from the flow parameters. Most of the calculations were performed for strain rates of 100 s^{-1}, but one set was carried to higher velocities where flame extinction occurred. The calculated value of a_p was 410 s^{-1}, and the corresponding value of χ_s was 16.7 s^{-1}. [35]

The limitations with regard to the use of potential flow conditions in opposed flow flame calculations continued to worry early workers in the area. It was recognized that most opposed jet configurations were designed to generate plug flows either through the use of nozzles or active flow straighteners. In other words, the radial velocities at the burner exits were set to be zero with both a and b also equal to zero at these locations. Furthermore, the nozzles had finite diameters as opposed to the infinite diameters assumed in the model. In 1988 Kee et al. demonstrated that it was possible to derive a pseudo one-dimensional similarity transform for problems which relaxed the condition imposed by the assumption of potential flow that b_p and a_p be constant throughout the isothermal region of the flow. [43] In their formulation, it is only required that the radial velocity profile vary linearly with radial position for a given axial position as opposed to having a constant value. Thus b is allowed to vary along the primary flow direction. This approach allows the case of initial plug flows, i.e., $\partial v / \partial r = \partial u / \partial r = 0$ at the burner exits, to be evaluated. The price paid for relaxing the potential flow boundary conditions was that the strain rate element normal to the flame surface, a, was no longer a constant for regions outside of the reacting boundary layer, but now varied with the similarity coordinate. Thus there was no longer a single strain rate which could be used to characterize the flow field. Kee et al. used the approach to calculate the structure of opposed flow premixed methane/air flames.

The formulation used by Kee et al. [43] is related to earlier work by Seshadri and Williams [44] who considered flow in a two-dimensional channel. Their results can be used to derive a characteristic global strain rate, a_g, for the pseudo one-dimensional flow, which is written for axisymmetric flow as

$$a_g = \frac{-2u_o}{L}\left[1+\frac{u_f}{(-u_o)}\sqrt{\frac{\rho_f}{\rho_o}}\right] \quad , \qquad (12)$$

where L is the separation distance of the two burners, u_f and u_o are the fuel and oxidizer velocities which have opposite signs for the opposed flow, and ρ_f and ρ_o are the fuel and oxidizer densities. This corresponds to the strain rate which would exist at the stagnation point for opposed flows if the boundary layer were infinitely thin. Flow fields with comparable values of a_g are expected to have similar spatial variations of velocity. It should be mentioned that Eq. (12) is occasionally found in the literature without the factor of 2. The form of Eq. (12) is correct for axisymmetric opposed flows.

Chelliah et al. [39] extended the formulation provided by Kee et al. [43] to treat opposed flow diffusion methane/air diffusion flames. Calculations were made for two different boundary conditions corresponding to either potential flow with a characteristic strain rate of a_p for the boundaries located at $x = 0$ and $x = L$ or plug flow conditions with strain rate $a(x = 0, x = L) = 0$ s^{-1} at the burner exits. An important feature of this work was comparison of the calculational results with detailed experimental measurements of the velocity field. The flows were generated by nozzles and were expected to be closely top hat in shape. Therefore, plug flow conditions at the burner exits would be expected to provide better agreement with experiments. This was indeed found to be the case, although small disagreements were still observed.

Recall that plug flow conditions at the burner exits require that a varies with axial location. The global strain rate given by Eq. (12) is one means for quantification. However, the reacting boundary layer is known to have a finite thickness, and the volume expansion associated with the heat release causes a to vary rapidly through the combustion region. As a result, the value of a at the stagnation plane does not actually correspond to a_g. For this reason, the measured value a on the oxidizer side of the flow just outside of the boundary layer, a_o, has been suggested for use as the characteristic strain rate for opposed-flow diffusion flames formed by plug flows. Chelliah et al. found that the values of a_g and a_o differed significantly. [39]

The calculations of Chelliah et al. were carried to high enough velocities to cause extinction of the flame. [39] For plug flow exit conditions the corresponding values of a_g and a_o at extinction were 610 s^{-1} and 391 s^{-1}, respectively, while the experimental value of a_o was 380 s^{-1}. Values of χ_s at extinction were also determined from the calculations. Interestingly, these values were nearly independent of the exit flow conditions, being roughly 14.7 s^{-1} in both cases. The experimental value was reported as 19.9 s^{-1}.

The existence of the various definitions of characteristic strain rates, i.e., a_p, a_g, and a_o have resulted in some confusion in the literature when different experiments and calculations are considered. Fisher et al. have compared values of a_o measured in a propane/air counterflow diffusion flame with the corresponding oxidizer air flow rates and values of a_g. [45] In each case, a linear relationship was found. This suggests that for a given flow configuration, values of a_g and a_o should be related by a constant.

Early calculations involving opposed flow diffusion flames assumed the combustion occurred adiabatically and did not allow for the possibility of radiative heat loss. Recently, however, detailed chemical kinetic calculations for methane/air diffusion flames have begun to appear in which the effects of radiation from combustion gases have been included. [46,47,48] The study by Maruta et al. considered laminar diffusion flames in the opposed jet configuration burning nitrogen-diluted methane. [46] Both detailed chemical kinetic modeling and experiments were reported. The experiments were performed in microgravity so that buoyancy effects on the flame were minimal. Their results showed that at high strain rates flame extinction was due primarily to strain effects. However, as the strain rate was lowered, the percentage of heat loss by radiation increased rapidly, lowering the flame temperature and ultimately extinguishing the flame. As a result of these

competing effects, plots of maximum flame temperature versus strain rate showed a maximum and plots of strain rate at extinction as a function of methane concentration in the fuel were double valued.

For their investigation, Chan et al. used a different modeling approach. [47] Their calculation is based on a steady-state laminar flamelet model which is solved in mixture fraction coordinates. The effects of strain were incorporated indirectly by varying χ_s. Both detailed chemical kinetics and radiation losses were included. These authors considered a methane/air diffusion flame. Their findings are consistent with those of Maruta et al. [46] The effects of radiation were minimal at high strain rates and extinction occurred due to the well known strain-rate mechanism. Extinction was calculated to take place at $\chi_s = 18.4\ s^{-1}$, and the maximum flame temperature at extinction was 1773 K (1771 K with radiation losses included). However, as the strain rate was lowered, the percentage of the total heat release rate loss due to radiation increased dramatically. Calculations without radiation indicated a continual increase in maximum temperature with decreasing χ_s, while the inclusion of radiation resulted in maximum temperatures which first increased, but then began to fall for values of $\chi_s < 2.5\ s^{-1}$. The falling temperature ultimately led to a second extinction at $\chi_s = 0.029\ s^{-1}$.

Gore et al. also found that radiation effects became more important at low strain rates. [48] Their calculations showed that there is a substantial range of strain rate for which the effects of strain rate and radiation losses nearly cancel, resulting in maximum flame temperatures which are roughly independent of strain rate.

There have been a number of investigations which have used detailed kinetic modeling to study flame inhibition and extinction processes. Most of these have involved the reduction of premixed flame speed due to the introduction of various inhibitors. Examples include the early studies of Westbrook [49,50,51] as well as a number of more recent works. [52,53,54,55] Very recently, inhibited flames studies have been extended to laminar opposed flow diffusion flames. [55,56,57,58,59]

Despite the large number of detailed kinetic modeling studies dealing with inhibition and extinction of flames by various agents, we have identified only one study which systematically considered the effects of inert thermal agents on a combustion system. Tuovinen calculated the structure of methane/air premixed flames in a well-stirred reactor with added CO_2, H_2O, N_2, and He. [60] The author found that the extinguishing capability of these compounds was proportional to the heat capacity of the gases. The temperatures at extinguishment using the various agents were within 50 K for a given stoichiometric ratio, φ (a range of φ = 0.7 - 1.2 was studied).

B. Modeling Approach

The current investigation seeks to calculate the effects of adding thermal agents to the air side of laminar opposed flow diffusion flames. There are a number of codes described in the literature for making these calculations. We desired to utilize a widely used code which was easily accessible to researchers. The code Oppdif [61] developed by Sandia National Laboratories was chosen. This code is now available commercially from Reaction Design[1] of San Diego, CA. Oppdif is built on a number of general purpose subroutines, collectively known as Chemkin-III [62], which handle many of the tasks associated with the calculation. Data describing the reaction mechanism and thermodynamic and transport properties are either incorporated in Oppdif or accessed as databases.

---

[1]Certain commercial equipment, instruments, or material are identified in this paper in order to adequately specify the experimental procedure. Such identification does not imply recommendation or endorsement by the National Institute of Standards and Technology, nor does it imply that the materials or equipment are necessarily the best available for the purpose.

Oppdif solves the psuedo-one-dimensional equations describing an axisymmetric opposed flow laminar diffusion flame. The equations are those originally reported by Kee et al. [43] for premixed flames to solve problems in which b is constant at the boundaries and was later extended to diffusion flames by Chelliah et al. [39] This includes the case of plug flows, i.e., $b = a = 0\ s^{-1}$ at the burner exits, which was used for all of the calculations which follow.

A detailed chemical kinetic mechanism is required to model the flame. After reviewing the literature, we chose the widely used methane/air mechanism developed with the support of the Gas Research Institute. The version used was GRI-Mech 1.2. [63] There is a later version of the mechanism, GRI-Mech 2.11, which contains nitrogen chemistry. The earlier version was chosen for use since NOX formation is not of interest to the current investigation.

GRI-Mech 1.2 consists of 32 chemical species undergoing 177 reactions. One- and two-carbon species are included. Thermodynamic and transport data are provided as separate files. The mechanism was created by starting with appropriate estimates for the rate constants and then optimizing the mechanism to provide the best agreement with experimental measurements in such systems as premixed flames, shock tube studies, and flow reactor investigations. [63] Note that the mechanism was not optimized using diffusion flame results.

Oppdif was mounted on a Silicon Graphics Incorporated Origin 200 workstation. An initial test for a laminar hydrogen/air opposed flow diffusion flame yielded good agreement with the solution provided in the documentation. By simply replacing the mechanism provided for the hydrogen/air flame with GRI-Mech 1.2, we were able to obtain an initial solution for a methane/air diffusion flame.

The purpose of our calculations is to determine extinction behavior for the flame as a function of flow conditions and agent concentration and to use this information to better understand the effectiveness of thermal agents for extinction of diffusion flames. Extinction of diffusion flames can be understood in terms of the "S" curve which was originally described by Fendell [64] and Liñán [65]. The name refers to the shape of a plot of maximum flame temperature versus Damkohler number, *Da*, where *Da* is the ratio of a characteristic flow mixing time and a characteristic combustion reaction time. The unique shape results from the highly nonlinear temperature dependence of combustion reactions. These authors showed that there were two possible solutions for mixtures of fuel and air—combustion and very slow reaction regimes. These two branches are connected by an unstable third branch which forms the central part of the "S", but is not physically observable. Starting well up on the burning branch, it is found that the maximum flame temperature decreases with decreasing *Da*. As the *Da* is decreased still further, the temperature begins to drop faster and is ultimately predicted to curve onto the middle branch and continue to fall off with increasing *Da*. Such a dependence on *Da* is physically unrealistic, and, as a result, the real flame system drops to the lower branch at the turning point. This is interpreted as flame extinction. A similar behavior applies to ignition. Starting on the lower branch, as the temperature is increased the reaction rate increases very slowly at first. However, a temperature is eventually reached where the rate begins to increase quickly and ultimately begins to increase with falling *Da*, passing onto the middle branch. However, due to the instability of this branch, the system actually jumps rapidly up to the burning branch. This is the process of spontaneous ignition.

For this study, the goal is to determine the flow conditions necessary to cause extinction of a flame formed by fuel and either air or air with added agent. Thus the problem becomes one of identifying the turning point for a plot of temperature versus *Da*. Either the velocity, appropriate characteristic strain-rate, or stoichiometric scalar dissipation rate can be used as the dependent variable, and since the mixing time associated with these parameters is inversely related to their values, the curve is reversed from that for a *Da* plot, with the maximum flame temperature decreasing with increasing velocity, characteristic strain rate, or scalar dissipation rate.

Early calculations of flame extinction simply increased the controlling parameter for burning solutions until further increases resulted in a nonburning solution (e.g., see [35]). Due to the rapid changes in temperature with flow parameters near the extinction point, solutions of opposed flow diffusion flames can become unstable, and there may be some uncertainty associated with the extinction value. As a result, so-called continuation methods have been implemented which allow calculations to be extended onto the unstable solution branch. [66,67] In this way it is possible to determine the turning point corresponding to extinction unambiguously.

Unfortunately, continuation approaches are not implemented in Oppdif. For this reason, we chose to employ the direct approach in which higher and higher flow velocities were used until either a nonburning solution was found or the differential solver was unable to find a solution. In order to minimize the associated uncertainties, very small incremental increases in velocity were utilized near the extinction point (the solver is more efficient when an earlier solution for similar conditions is used as the starting point). An arbitrary, but stringent, criterion was adopted which defined the extinction velocity as that for which a burning solution was still obtained, but for which an increase of only 0.01 cm/s in the fuel and air initial velocities either resulted in a failure to find a solution or a nonburning solution. Additional small increases in velocity always resulted in nonburning solutions. As we shall show, plots of maximum flame temperature versus the controlling parameters (e.g., velocity) indicate that the flames were indeed near the extinction point as reflected by large temperature drops for small changes in the control parameter. It is believed that this approach results in small errors for estimates of the calculated extinction condition.

A number of parameters are relevant to Oppdif calculations. [61] Many of these are summarized in Table 7. The general procedure was to find a solution for a methane/air diffusion flame by first solving an isothermal case and using the solution as the input for a calculation in which the energy equation was added. Once a solution was available, it could be used as the starting point for calculations in which such parameters as the oxidizer and flow velocities were changed. Only the formulation including the energy equation was solved for the "restarted" cases. The new solution then became the starting point for cases involving further changes in the controlling parameters. Oppdif allows the grid for the calculations to be adapted to best match the latest solution. This feature was used frequently for these calculations. Normally, between 130 and 150 grids points were used for a final solution. For simplicity, the opposed (i.e., opposite signs for velocity) fuel and oxidizer exit velocity magnitudes were always set equal to each other. The exit temperatures were 300 K.

The final solutions for a particular problem were saved in binary files. A program named Postopp was supplied by Reaction Design [61] which reads these files and generates ASCII files containing such parameters as temperature, density, fuel mixture fraction, axial and radial velocities, and axial and normal strain rate elements a and b as functions of distance from the fuel nozzle (z = 0 cm). This program was modified to also output the largest absolute value a on the oxidizer side, a_o, the stoichiometric mixture fraction, and the scalar dissipation rate at the location corresponding to a stoichiometric mixture fraction. The derivatives required in Eq. (11) were calculated by simple forward differencing of mixture fraction values, and values of D were corrected for variations in the local temperature using the expression recommended by Norton et al. [68]

Figure 1 shows a plot of maximum temperature, T_{max}, versus flow velocity (equal magnitudes for the fuel and oxidizer opposed velocities) calculated for a laminar opposed flow methane/air diffusion flame. The fuel is 100% methane and air is assumed to be composed of 78.1% N_2, 21.0% O_2, and 0.9% Ar. As expected, T_{max} decreases with increasing velocity. Extinction occurs for a velocity of 320.12 cm/s for a maximum flame temperature of 1785 K. A global strain rate, a_g, of 558 s^{-1} is calculated for the extinction condition using Eq. (12). Puri and Seshadri [69] have reported an experimental value for a_g of 542 s^{-1} while Chelliah et al. [39] measured a value of a_g = 610 s^{-1} The calculated value is in reasonable agreement with these results.

Table 7. Some Parameters Used in Most Oppdif Calculations

Keyword	
ENRG	Energy Equation Included
NOFT	Skip the Fixed Temperature Problem
RSTR	Restart From Earlier Solution
IRET (retirement period)	20
RTOL (relative convergence for Newton's method)	1.E-3
ATOL (absolute convergence for Newton's method)	1.E-6
ATIM (absolute convergence for timestepping)	1.E-6
RTIM (relative convergence for timestepping)	1.E-3
XEND (physical length)	2 cm
TFUE , TOXI (fuel and oxidizer initial temperatures)	300 K
PRES	1 atmosphere
AFUE, AOXI (radial gradient at inlet)	0 s^{-1}
MIX	Mixture-Averaged Formula for Diffusion Velocities

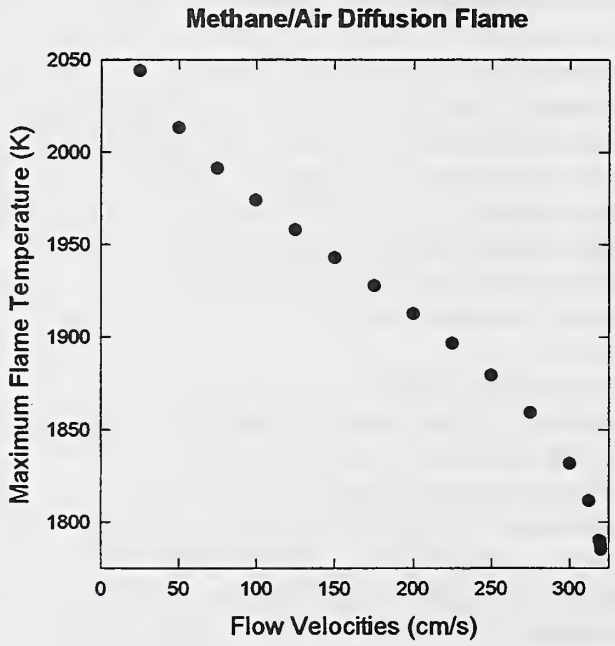

Figure 1. Maximum flame temperature plotted as a function of the equal fuel and air velocity magnitudes for a methane/air opposed flow diffusion flame.

Figure 2 shows two examples, one for relatively low fuel and air velocity magnitudes and one for a flame very close to extinction, of the variation of the local characteristic strain rate, a, with position. Several interesting behaviors can be seen. First, as expected, absolute values of a are higher for the case with higher initial

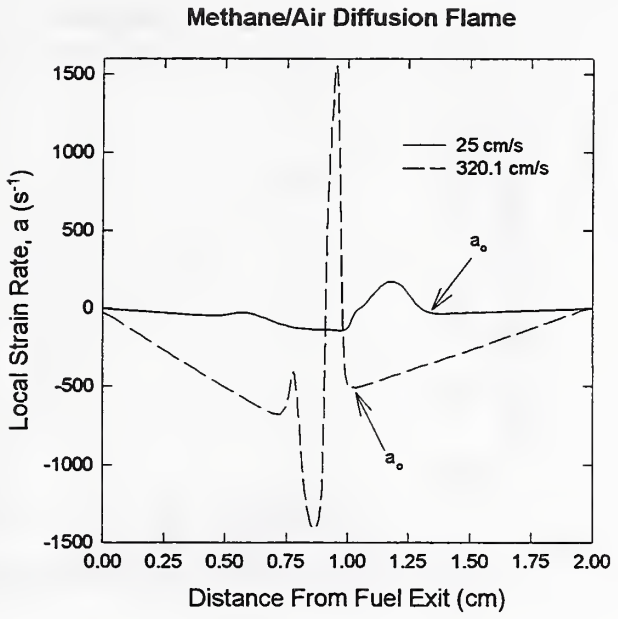

Figure 2. Calculated strain rates, *a*, are plotted as a function of distance from the fuel exit for low exit velocity magnitudes (25 cm/s for fuel and air) and for a condition very close to extinction (320.1 cm/s).

velocities. For regions outside of the boundary layer, a values increase or decrease roughly linearly with increasing position, but large intense variations are evident in the vicinity of the flame front. These large fluctuations within the flame zone result from the volume expansion due to heat release. It is clear that the boundary layer width for the low velocity case is considerably broader than for the higher flow velocity. This is expected since higher absolute velocities should more effectively overcome the effects of molecular diffusion and result in a narrower mixing layer.

The first maximum in the absolute value of a on the oxidizer side (see Figure 2) can be taken to be the largest value outside of the boundary layer, i.e., $|a_o|$. Figure 3 shows a plot of maximum flame temperature versus $|a_o|$ for the various flow velocities. As expected, the maximum flame temperature decreases with increasing $|a_o|$. Extinction is calculated to occur when $|a_o|$ is increased to 509 s^{-1}. Three experimental measurements of $|a_o|$ at extinction are available in the literature for methane/air diffusion flames. Chelliah et al. reported extinction for $|a_o|$ = 380 s^{-1} [39], Papas et al. report (405 ± 25) s^{-1} [33], and Du and Axelbaum report (375 ± 10) s^{-1} [70]. These values should be considered equal within experimental uncertainty. The value calculated here is roughly 30% higher. Two possible reasons for this are different boundary conditions in the experiment and model and the possible dependence of the results on chemical mechanism. Reasons for the difference are discussed further below.

Figure 4 shows the mixture fraction, i.e., the fraction of the mass of the combustion mixture derived from fuel, plotted as a function of distance from the fuel source for the two same conditions used for Figure 2. The narrowing of the boundary layer due to increased strain rate is clearly evident. The shape of the curve becomes more asymmetric as the velocity decreases. Since values of the mixture fraction are now available, it is

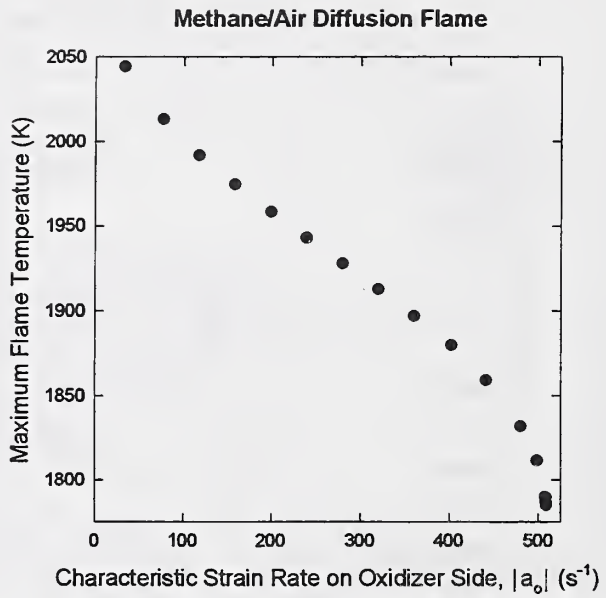

Figure 3. The maximum flame temperature is plotted against a characteristic local strain rate, $|a_o|$, defined to be equal to the highest absolute value of a on the air side observed outside of the boundary layer associated with the flame.

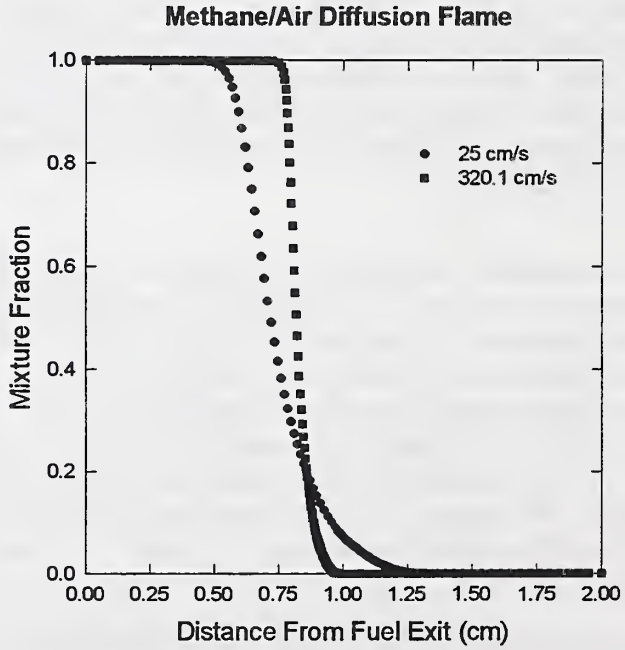

Figure 4 Mixture fraction is plotted as a function of distance from the fuel exit for low exit velocity magnitudes (25 cm/s for fuel and air) and for a condition very close to extinction (320.1 cm/s).

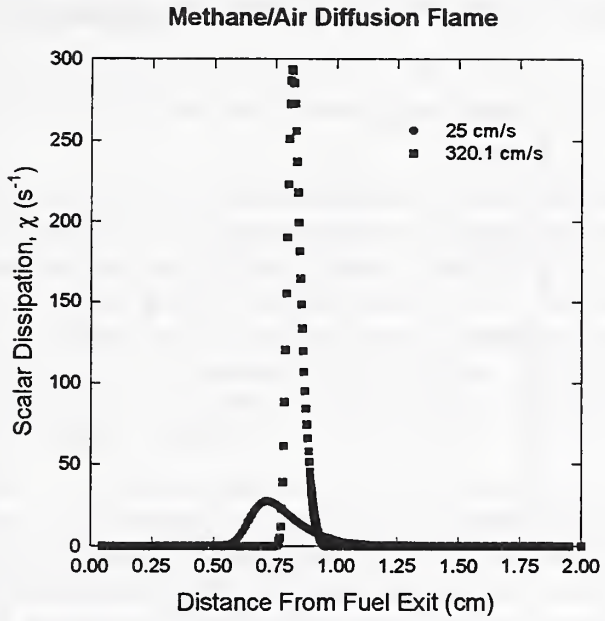

Figure 5. Calculated scalar dissipation rates, χ, are plotted as a function of distance from the fuel exit for low exit velocity magnitudes (25 cm/s for fuel and air) and for a condition very close to extinction (320.1 cm/s).

possible to calculate the scalar dissipation rate, χ, as a function of x using Eq. (11). Figure 5 shows the results, which demonstrate the strong dependence of χ on the flow velocities. The value of χ at the stoichiometric surface, χ_s, can now be determined by interpolating the results to find the value of χ for a mixture fraction of 0.055, the stoichiometric value. The results are $\chi_s = 1.70\ s^{-1}$ and $\chi_s = 20.7\ s^{-1}$ for fuel and air exit velocity magnitudes of 25 cm/s and 320.1 cm/s, respectively.

In Figure 6 maximum calculated flame temperatures are plotted as a function of χ_s for a series of methane/air flames in which the fuel and air velocities were varied. The temperature drops with increasing χ_s, and extinction is calculated to occur for $\chi_s = 20.7\ s^{-1}$.

In order to obtain insights into the effect of the separation of the fuel and oxidizer sources, calculations were also performed for $L = 1.0$ cm. Table 8 compares the various measures used to quantify extinction for the two sets of calculations and includes the maximum flame temperature at extinction. While the initial flow velocities required for extinguishment depend strongly on L, the various measures for the effects of strain vary only slightly for the two cases. These minor differences are most likely due to the variations in the grids used for the calculations. These limited results suggest that for the assumed initial conditions, i.e., no radial gradients at the fuel and air exits, the velocities of fuel and air required for extinction are roughly proportional to L, while the various measures used to describe the role of strain are roughly independent of L.

It is of interest to compare the results of the current calculations with comparable modeling results found in the literature. Parameters used to characterize methane/air diffusion flames near extinction are included in Table 8 for a number of studies. Substantial variations are evident for calculated extinction parameters in terms of a_g, $|a_o|$, and χ_s. The three sets of results for Tanoff et al. provide a strong clue as to a possible reason for these

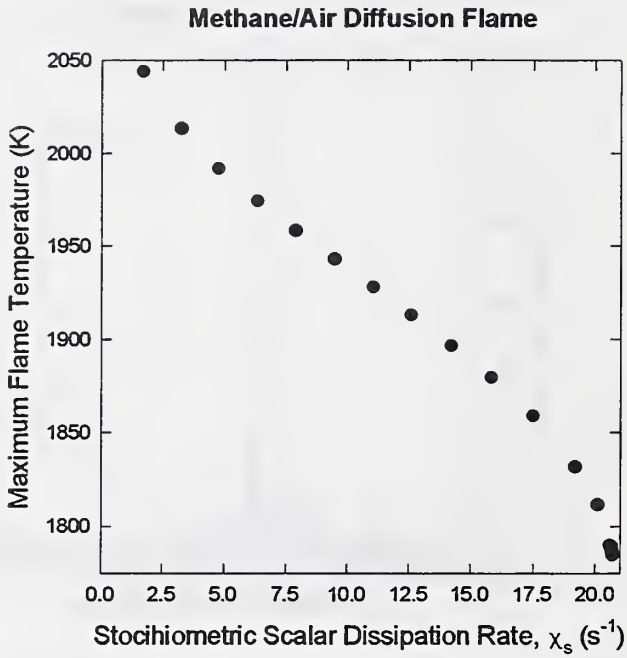

Figure 6. Values of maximum flame temperature for opposed-flow methane/air diffusion flames are plotted as a function of χ_s which is varied by changing the velocities of the fuel and air. Extinction is calculated to occur for $\chi_s = 20.7\ s^{-1}$.

Table 8. Various Measures of Strain Rate Calculated for the Methane/Air Diffusion Flame at Extinction

Source	L (cm)	u_f (cm/s)	u_o (cm/s)	a_g (s^{-1})	$\lvert a_o \rvert$ (s^{-1})	χ_s (s^{-1})	T_{max} (K)
This Work	1.0	157	-157	547	500	19.9	1792
This Work	2.0	320	-320	558	509	20.7	1785
Dixon-Lewis et al.[35]	1.0	-	-	-	-	16.7	1769
Chelliah et al.[39]	1.0	185	-135	610	391	14.7	1758
Du and Axelbaum[70]	0.8	-	-	-	494	-	1770
Tanoff et al.[57]	-	-	-		350	-	1808
Tanoff et al.[57]	-	-	-	-	490	-	-
Tanoff et al.[57]					585	-	-
Chan et al.[47]	-	-	-	-	-	19.4	1773
Lentati and Chelliah[58]	1.0	-	-	-	425	-	1790

variations. [57] The only changes between the calculations are that different detailed chemical kinetic mechanisms were used for each. Values of $|a_o|$ vary by nearly a factor of two. One of the mechanisms used by Tanoff et al. was GRI-Mech 2.11 which would be expected to provide similar results to the calculations reported here. The actual difference is roughly 15%. This is somewhat larger than expected. We are not able to provide an explanation for the discrepancy. The only other study which used GRI-Mech 2.11 was that of Chan et al. [47] Their value of $\chi_s = 19.4\ s^{-1}$ is quite close to those of 19.9 s^{-1} and 20.7 s^{-1} given in Table 8 for

the current investigation. We conclude that the current results are consistent with existing literature findings, but there is a relatively large uncertainty in the quantitative results which are sensitive to the detailed chemical mechanisms used.

C. Effects of Nitrogen Addition on Diffusion Flame Extinction and Extinguishment

The purpose of these calculations was to investigate the effects of thermal agents on the structure of opposed flow diffusion flames and to use the findings to gain insights into flame extinguishment by these agents. Note that we are purposefully distinguishing the meanings of flame "extinction" and "extinguishment". Extinction is used to describe a flame which goes out due to the local strain rate or other conditions causing the flame to become unstable. Flame extinguishment refers to the more specific conditions necessary to put out buoyancy-dominated flames which are expected to be characteristic of most fires. The cup burner test is an example of an experimental technique designed to characterize extinguishment. Thus flame extinguishment can be considered as a particular case of flame extinction.

In order to evaluate the effectiveness of the calculations, it is necessary to compare with experimental findings. The most appropriate measure for characterizing diffusion flame extinguishment is the amount of thermal agent required to extinguish a buoyancy dominated flame burning at standard gravity. This concentration is related to the concept of a limiting oxygen index (LOI), which is the lowest oxygen concentration which can support a flame under such conditions. The minimum agent amount required to meet this condition is sometimes referred to as the inerting concentration. Appropriate experimental data are often reported in terms of inerting concentrations or LOIs.

Despite the large number of studies previously reported for methane combustion, we were only able to identify three measurements which provided the LOI for methane flames burning in air with an added thermal agent. All three studied the effect of added nitrogen. Simmons and Wolfhard [71], Ishizuka and Tsuji [72], and Puri and Seshadri [69] reported LOI values for added nitrogen of 0.139, 0.143, and 0.15, respectively, which correspond to 33.8%, 31.9%, and 28.6% by volume nitrogen added to air. These three measurements are in reasonable agreement. Simple averaging of the two higher values yields an estimate of 33% which will be taken as the extinguishing concentration for nitrogen. Simmons and Wolfhard calculated the adiabatic flame temperature for a stoichiometric premixed flame corresponding to their extinction condition as 1820 K. Ishizuka and Tsuji used thermocouples to measure the maximum flame temperature in their diffusion flame as 1483 K for the LOI condition, while Puri and Seshadri recorded a value of 1595 K.

A series of calculations were performed for methane opposed-flow diffusion flames reacting with air containing various percentages of added nitrogen. Figure 7 shows the results. Several points are immediately obvious. As the percentage of added nitrogen increases, the fuel and oxidizer velocity magnitudes sufficient to cause flame extinction decrease. The maximum flame temperature at extinction also decreases with increasing nitrogen concentration. The negative slopes of the plots for T_{max} versus velocity increase in absolute value as the concentration of nitrogen increases.

The concentration of added nitrogen estimated to correspond to the experimental LOI is 33%. The value of T_{max} at extinction for this condition is 1545 K. This is very close to the experimental values of 1483 K and 1595 reported by Ishizuka and Tsuji. [72] and Puri and Seshadri [69], respectively. In fact, the agreement is probably better than a simple comparison indicates since the thermocouple measurements of Ishizuka and Tsuji were not corrected for radiative heat losses, which would be expected to decrease the measured temperature below the actual temperature. The thermocouple measurements of Puri and Seshadri were corrected for radiative heat losses. The calculated temperature is expected to be a slight overestimate due to neglect of radiative heat losses from flame gases.

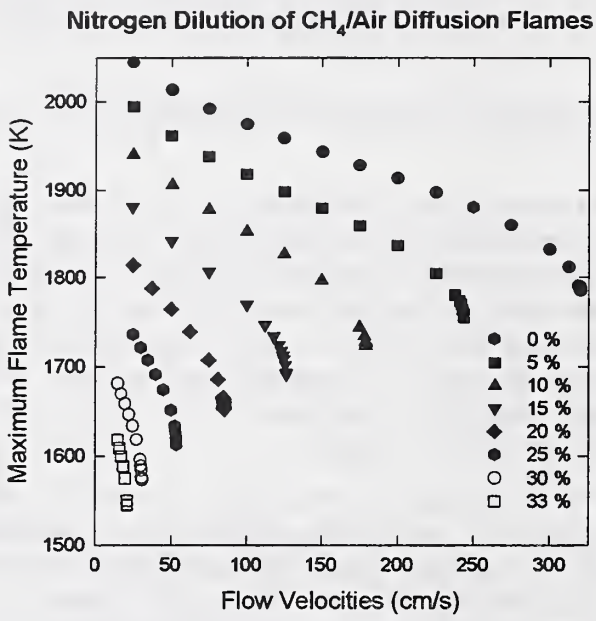

Figure 7. Maximum calculated flame temperatures are plotted against methane and oxidizer exit velocity magnitudes for a series of methane/air opposed flow diffusion flames diluted with nitrogen. Symbols correspond to the percentage of added nitrogen.

These estimates for the maximum flame temperature at extinguishment are consistent with others available in the literature. Sheinson et al. indicate that hydrocarbon combustion is not sustainable when the maximum flame temperature drops below roughly 1600 K. [73] This estimate is based upon work by Roberts and Quince. [74] Very recently, Babb et al. have reported flame temperature measurements in heptane flames near their extinguishment points using air diluted by N_2 and CO_2. [75] For both thermal agents maximum flame temperatures at extinguishment were on the order of 1500 K. Similar measurements using propane as fuel gave maximum flame temperatures of 1600 K and 1700 K for N_2 and CO_2, respectively.

For the conditions corresponding to the assumed LOI for nitrogen, the velocities of the fuel and air at extinction are calculated to be 21.42 cm/s. Corresponding values for the various measures used to characterize the flow condition at extinction are $a_g = 37.5\ s^{-1}$, $|a_o| = 27.0\ s^{-1}$, and $\chi_s = 0.80\ s^{-1}$. It is interesting to see how the various measures vary relative to each other with added nitrogen concentration. Figure 8 shows $a_g/|a_o|$, a_g/χ_s, and $|a_o|/\chi_s$ versus percentage of added nitrogen. It is clear that the three measures have different dependencies on the amount of thermal agent added. The reason for this is the variation in the thickness of the boundary layer as the flow velocities are changed. The dependence on concentration requires that great care be exercised when comparing results in terms of different measures of strain rate.

An important question is: what strain rate is appropriate to use when determining the minimum value of an added thermal agent required to extinguish buoyancy-dominated diffusion flames at normal gravity? The only discussion of this point of which we are aware was presented by Hamins et al. [76] These authors compared cup burner measurements (heptane fuel) of extinguishing concentrations for a variety of agents with corresponding measurements made in a counterflow flame. The counterflow measurements were made over a range of flow velocities which were characterized in terms of a global strain rate appropriate for the oxidizer flow impinging on a liquid surface. In agreement with the current calculations, the required strain rate to

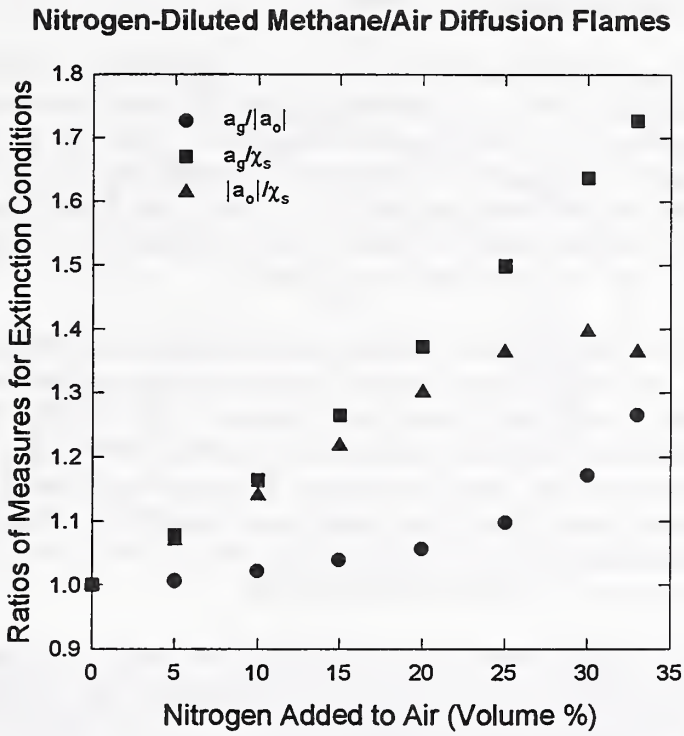

Figure 8. Ratios for the indicated measures of conditions at flame extinction are plotted as a function of the percentage of nitrogen added to the air for methane/air flames.

cause extinction of the counterflow flame decreased with the concentration of added agent. When the concentration of added agents for the opposed flame were comparable to those observed in the cup burner test, the global strain rate was on the order of 50 s^{-1}. Due to the different boundary conditions and fuels used between the current investigation and those for Hamins et al., as well as slightly different definitions for the global strain rates, direct quantitative comparisons are not appropriate. However, it is clear that the strain rates have comparable magnitudes in each case. It is important to note that the strain rate appropriate for characterizing the LOI is much lower than typically used for experimental and modeling investigations of opposed-flow laminar diffusion flames. In their early work, Puri and Seshadri reported that extinguishment by nitrogen added to air occurred when a_g was decreased to approximately 50 s^{-1}. [69]

It is interesting to speculate as to why lower and lower strain rates can not be sustained for the flames at normal gravity. The most likely reason is that buoyancy effects result in a lower limit for the minimum strain rate element perpendicular to a flame surface. Buoyancy always accelerates hot combustion gases relative to the cold oxidizer with the result that the flame surface will be subject to a nonzero perpendicular strain rate. The results of Hamins et al. [76] and the current findings suggest this minimum strain rate is on the order of a few tens of inverse seconds.

D. Effects of Argon Addition on Extinction and Extinguishment of Methane Diffusion Flames Burning in Argon "Air"

As already pointed out, we have identified no additional measurements of LOI for thermal agents added to methane/air diffusion flames. However, Ishizuka and Tsuji did make measurements for methane burning in an artificial "air", consisting of 21% oxygen and 79% argon. [72] This "air" was diluted with argon until a LOI was found. The result corresponded to an added argon concentration of 54.3%. The measured maximum flame temperature for the LOI flame was 1443 K, or roughly 40 K less than for standard air diluted with nitrogen. In order to test the ability to predict LOI concentrations of added thermal agents, a series of calculations for argon "air" diluted with argon were made.

Figure 9 shows a plot of the maximum calculated flame temperature as a function of the percentage of argon added to the argon "air" and the equal fuel and oxidizer velocity magnitudes. Comparison with Figure 7 shows that replacing nitrogen with argon has a dramatic effect on the flame behavior. First, flame temperatures are considerably higher for given diluent concentration and fuel and oxidizer velocities for the argon "air". This is due to the lower heat capacity of argon as compared to nitrogen. As a result of the increase in temperature, much higher flow velocities are required to generate the characteristic strain rate necessary to result in extinction of the methane flame. For the same reason, higher concentrations of argon must be added to achieve the LOI than in the nitrogen case.

The flame formed by oxidizer diluted with 50% argon is calculated to undergo extinction with a maximum temperature of 1610 K and methane and oxidizer velocity magnitudes of 37.8 cm/s. The corresponding results for 54% argon, corresponding to the experimental LOI, are 1473 K and 15.9 cm/s. These values are both slightly smaller than found for the methane/air flame diluted with nitrogen, 1545 K and 21.4 cm/s, respectively. However, they are remarkably close when one recalls that the use of argon instead of nitrogen should result in a significantly different flame structure due to changes in heat capacity and thermal diffusivity on going from nitrogen to argon. In fact, if one simply assumes that the LOI occurs for the same maximum flame temperature, i.e., roughly 1550 K, as for the nitrogen-diluted air flame, it is possible to estimate the required argon concentration as 52% from Figure 9. This is only 4% less than the experimental value. Thus, assuming that the LOI corresponds to the added concentration necessary to reduce the maximum calculated flame temperature at extinction to 1550 K should provide an excellent estimate for the percentage of an arbitrary thermal agent required to extinguish a fire. This estimation method is similar to the approach suggested by Sheinson et al. [73]

E. Calculated Extinguishing Concentrations for Several Gaseous Thermal Agents

Opposed flow diffusion flame calculations have been used to estimate the required extinguishing concentration, i.e., the added concentration corresponding to the LOI, for a number of gases which are expected to act primarily as thermal agents. Figures 10-13 show plots of the maximum calculated flame temperature as a function of the fuel and oxidizer velocity magnitudes, where air has been diluted by the indicated percentages of argon, helium, carbon dioxide, and water, respectively. It should be noted that both water and carbon dioxide are products of methane combustion and could conceivably modify the combustion chemistry slightly. However, both are believed to act primarily as thermal agents. For water, the vapor pressure at the lower temperatures is less than required to generate the concentrations assumed in the calculations. As an example, at 300 K the water vapor pressure is 3.57 kPa, which corresponds to a mole fraction of 0.035 in atmospheric air. Therefore, for temperatures near 300 K, the higher water vapor concentrations are assumed to be supersaturated.

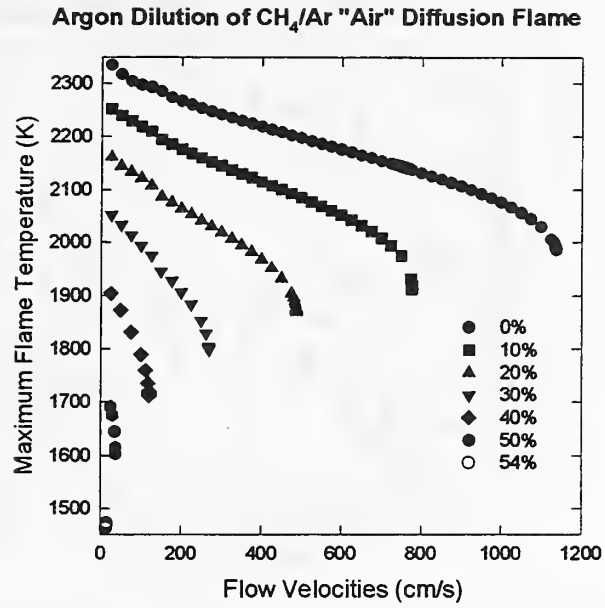

Figure 9. Maximum calculated flame temperatures are plotted against methane and oxidizer flow velocity magnitudes for a series of methane/argon "air" opposed flow diffusion flames diluted with argon. Symbols correspond to the percentage of added argon.

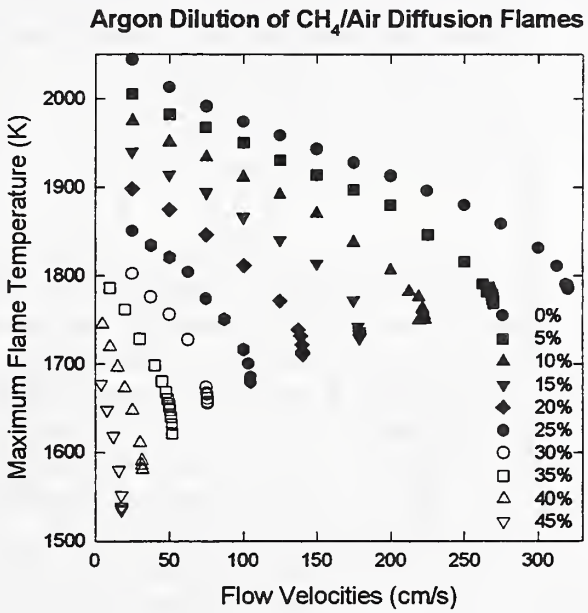

Figure 10. Maximum calculated flame temperatures are plotted against methane and oxidizer flow velocity magnitudes for a series of methane/air opposed flow diffusion flames diluted with argon. Symbols correspond to the percentage of added argon.

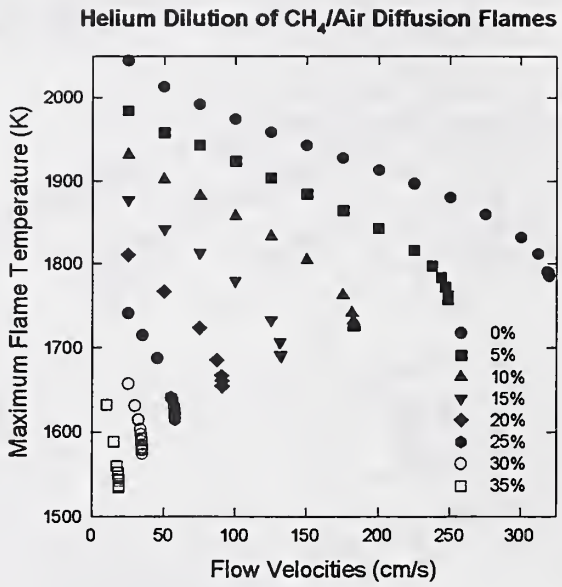

Figure 11. Maximum calculated flame temperatures are plotted against methane and oxidizer flow velocity magnitudes for a series of methane/air opposed flow diffusion flames diluted with helium. Symbols correspond to the percentage of added helium.

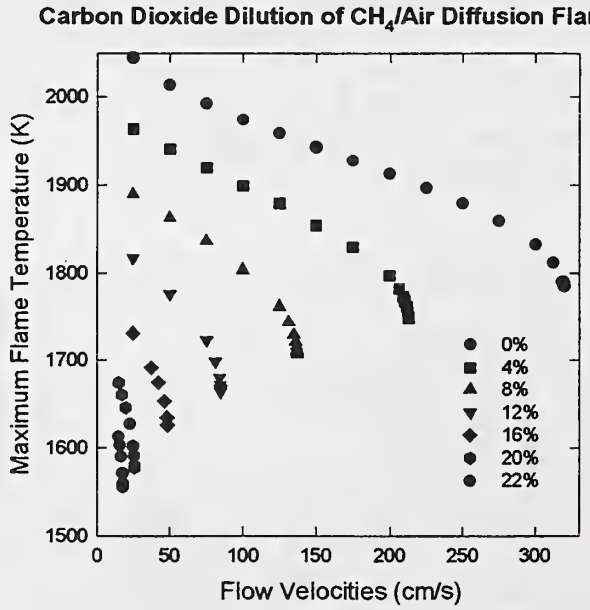

Figure 12. Maximum calculated flame temperatures are plotted against methane and oxidizer flow velocity magnitudes for a series of methane/air opposed flow diffusion flames diluted with carbon dioxide. Symbols correspond to the percentage of added carbon dioxide.

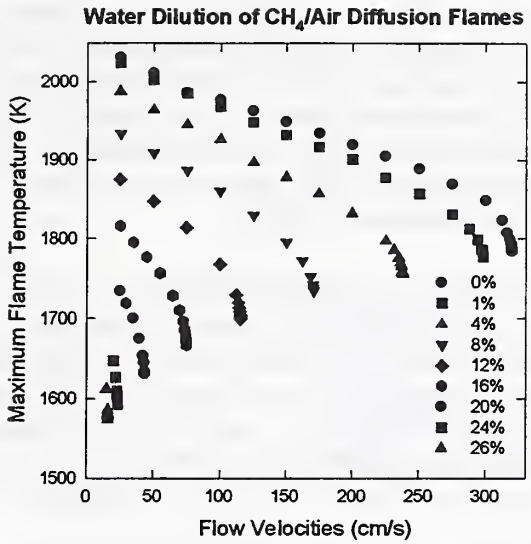

Figure 13. Maximum calculated flame temperatures are plotted against methane and oxidizer flow velocity magnitudes for a series of methane/air opposed flow diffusion flames diluted with water vapor. Symbols correspond to the percentage of added water vapor.

Table 9. Extinguishing Concentrations (Mole Fraction) of Thermal Agents

Thermal Agent	Current Work	Cup Burner [73]	Cup Burner [75]	Cup Burner [77]	Cup Burner [78]
Nitrogen	0.33	0.30	0.33	0.32	0.30
Argon	0.43	0.41	-	0.41	0.38
Helium	0.34	0.32	-	0.31	-
Carbon Dioxide	0.22	0.21	0.20	0.23	0.20
Water	0.28	-	-	-	-

By assuming the limit temperature is 1550 K, it is possible to estimate the extinguishing concentrations for each of these thermal agents. These estimates are tabulated in Table 9. As already discussed, the only experimental values for opposed flow methane diffusion flames we have identified for these agents are for nitrogen dilution. Cup burner determinations of extinguishing concentrations using heptane as fuel have been reported for some of these thermal agents by Sheinson et al. [73], Babb et al. [75], Hamins et al. [77] and Moore et al. [78] These values are included in Table 9 for comparison purposes. The maximum difference between values calculated for methane and the experimental values for heptane is 12%, with the vast majority being less than 10%. With the exception of carbon dioxide, the cup burner measurements are somewhat lower than for the counterflow flame. The differences between the cup burner and opposed flow flame results could be due to the use of different fuels or to differences in burner configuration. The heptane fires are burning just above a liquid fuel in a coflow of oxidizer, and it may be easier to blow out this type of flame than the opposed flow diffusion flame which is stabilized away from surfaces. The close tracking of the calculated results and the experimental findings suggests that detailed chemical kinetic modeling can accurately predict the amount of a thermal agent required to extinguish opposed flow diffusion and cup burner flames.

The differences in the extinguishing concentrations of helium and argon are interesting since these agents are both monatomic gases and have the same heat capacities. The difference is clear in both the calculations and the experimental values. The fact that helium is a more efficient extinguishing agent means that at least one other parameter, in addition to heat capacity, is important in determining extinguishing efficiency. A related observation was reported by Coward and Hartwell for the inerting of premixed flames and was attributed to the much higher thermal conductivity of helium which distributes the heat of combustion over a larger region of space and therefore weakens the flame. [79] The same explanation is most likely valid for diffusion flames. Sheinson et al. reached the same conclusion. [73]

Inspection of the various curves for the dependence of calculated maximum flame temperature on the fuel and oxidizer velocity magnitudes in Figs. 7 and 10-13 shows that for given velocities and extinction temperatures, they have very similar shapes. This is true despite the fact that the amount of added agent and, therefore, the oxygen concentration and stoichiometric ratio vary dramatically with agent. This is confirmed by Figure 14 which shows the maximum flame temperature at extinction as a function of fuel and oxidizer exit velocity magnitudes for the five thermal agents added to air as well as the results for argon added to argon "air". The data fall within a narrow band on either side of a well defined curve.

Closer inspection of Figure 14 shows that the data for argon "air" tend to fall at higher temperatures by amounts which decrease with dilution, while the water vapor data tend to lie near the top of the band by amounts which increase with dilution. The difference between adding argon to air and argon "air" is most likely due to the different physical properties of argon and nitrogen. Apparently, these differences are most important for high strain rates and are relatively minor at the lower strain rates typical of buoyancy-dominated diffusion flames. Recall that the estimated value of the extinguishing concentration for argon added to argon "air" was in good agreement with the experimental value of Ishizuka and Tsuji. [72] The increasing differences with decreasing strain rate for water may be due to two possible effects. The first is the higher thermal diffusivity expected for the relatively small water molecule. However, the results for helium, which has a much higher thermal diffusity, fall close to the results for nitrogen, argon, and carbon dioxide. The second possible explanation is that the water vapor slightly modifies the chemical structure of the flame and seems the more likely of the two. Increases in water concentration can interact with the flame chemistry through a number of reactions including the well known water-gas shift reaction,

$$H_2O + CO \Leftrightarrow CO_2 + H_2 \,. \qquad (13)$$

The addition of water to the oxidizer is expected to drive this equilibrium towards the right, resulting in additional heat release and a slightly higher temperature, as observed. The findings of Lentati and Chelliah indicate that water does display a small chemical effect. [59] Dilution with carbon dioxide would be expected to drive the equilibrium in Eq. (13) in the opposite direction, however, this effect on extinguishment must be small since the carbon dioxide results lie very close to those for nitrogen, argon, and helium.

Simply plotting the results in terms of the exit velocity magnitudes of methane and oxidizer at extinction leads to a collapse of the results for different thermal agents to a well defined curve. It is of interest to see if the collapse is improved by plotting the data in terms of the global strain rate given by Eq. (12), a_g, or the maximum absolute value of the characteristic strain rate element on the oxidizer side lying outside of the boundary layer, $|a_o|$. Figure 15 and Figure 16 show the data plotted in terms of these two characteristic strain rates. The overall appearances of the two plots are very similar to Figure 14, which is simply in terms of the exit velocities. For this reason, further discussion is based only on the flow velocity magnitudes for methane and oxidizer.

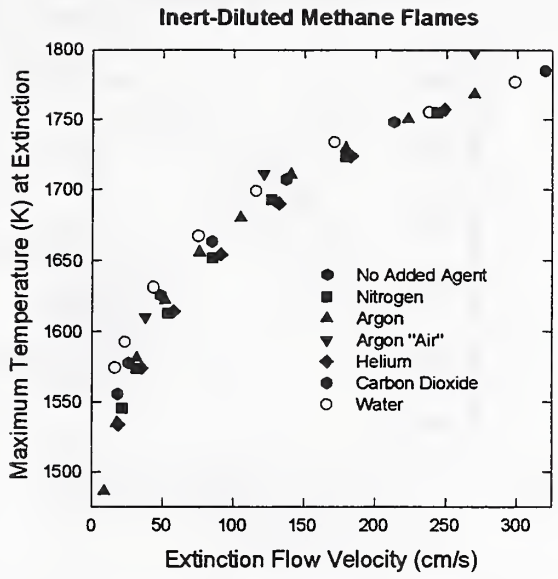

Figure 14. Values of maximum flame temperature at extinction are plotted as a function of the corresponding fuel and oxidizer velocity magnitudes for a range of concentrations of various thermal agents.

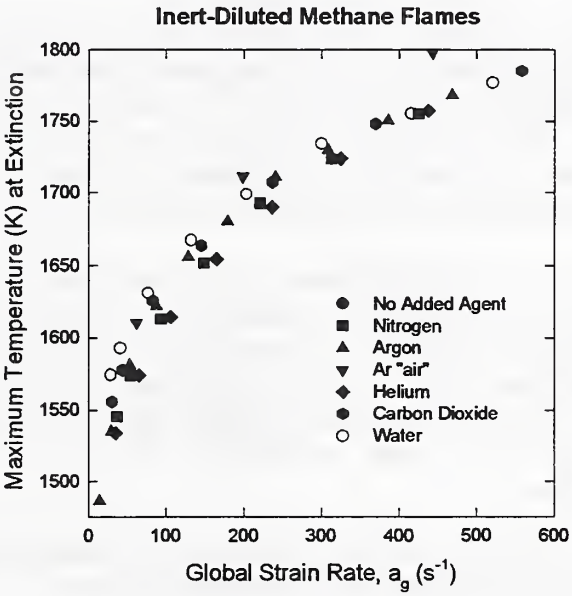

Figure 15. Values of maximum flame temperature at extinction are plotted as a function of the corresponding global strain rates, a_g, for a range of concentrations of various thermal agents.

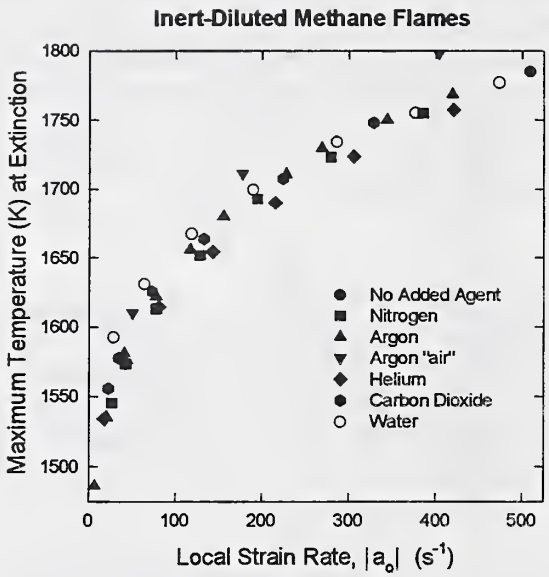

Figure 16. Values of maximum flame temperature at extinction are plotted against the corresponding characteristic local strain rates, $|a_o|$, defined as the highest absolute value of strain rate observed outside of the boundary layer on the oxidizer side of the flame, for a range of concentrations of various thermal agents.

A more quantitative idea of the degree of correlation between the maximum calculated flame temperatures at extinction and the fuel and oxidizer flow velocity magnitudes is obtained from Figure 17 where the results for N_2, Ar, He, and CO_2 addition have been consolidated and fit to two piecewise fourth order polynomials on either side of 105 cm/s. The resulting fits are drawn as a solid line. The coefficients of determination for the nonlinear curve fits were 0.97 and 0.98, which indicate a high degree of confidence in the fits. The polynomials can be used to predict values of maximum temperature for given exit velocities.

To determine if there is a relationship between added agent concentration and the calculated maximum temperature at extinction, the temperatures were plotted versus the ratio of the percentage of added agent and that required for extinguishment as shown in Figure 18. The results for argon added to argon "air" lie well away from the remaining data. The trend of less effectiveness of water vapor at low velocities is also evident. While the data partially collapse for the remaining agents, the spread indicates that simply calculating a single extinction condition for a single agent concentration will not suffice for predicting the extinguishing concentration for that agent.

F. Effects of Dilution and Heat Extraction Location Relative to the Flame Front on Extinction and Extinguishment of Diffusion Flames

An important advantage of modeling investigations is the ability to perform calculations for conditions which are not physically possible in order to learn details concerning the role of various system parameters. One question which has been the subject of speculation is the relative importance of heat extraction and dilution on the effectiveness of a thermal agent. Here dilution effects refer to any role of a thermal agent which is not simply due its ability to extract heat. In order to obtain insights into this behavior, an artificial agent was

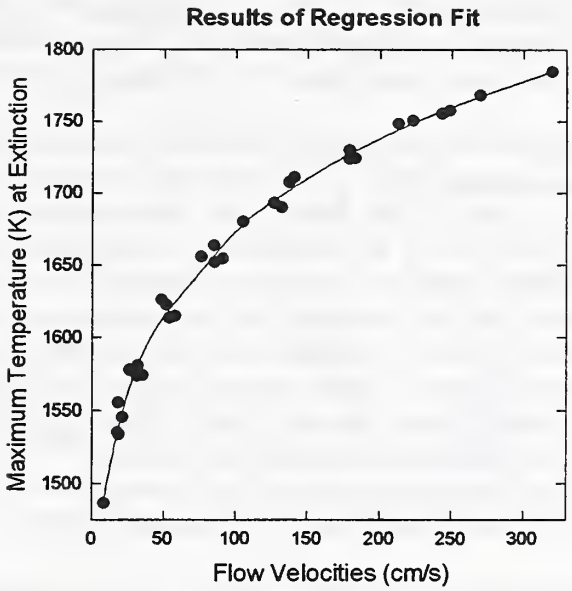

Figure 17. Maximum flame temperatures at extinction for N_2, Ar, He, and CO_2 as a function of the corresponding fuel and oxidizer velocity magnitudes are fit by two piecewise fourth order polynomials (solid line).

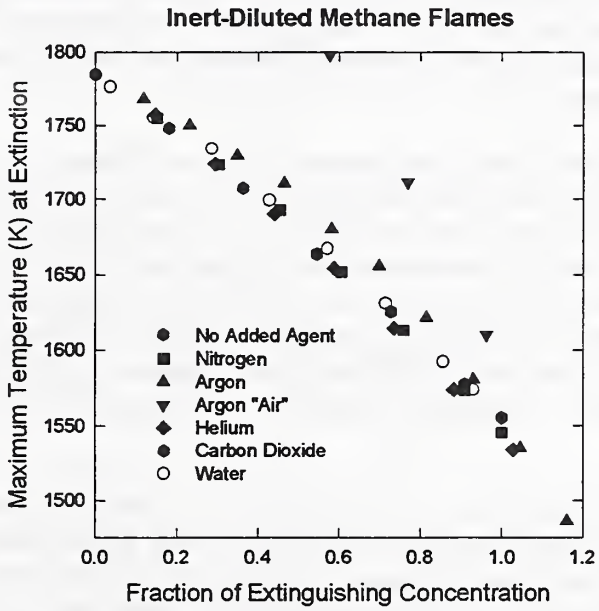

Figure 18. The maximum temperature at extinction for counterflow methane flames is plotted as a function of the percentage of a thermal agent added to air divided by the amount calculated to be required for flame extinguishment.

created by starting with argon and setting its heat capacity to zero. Direct comparison with the results for added argon allows the relative roles of heat extraction and dilution to be characterized. Sheinson et al. have discussed the effects of dilution on extinguishment. [73] They concluded that they are relatively small compared to direct heat removal due to heat capacity for the thermal agents CF_4 and SF_6.

Figure 19 is a plot of calculated maximum flame temperature versus fuel and oxidizer velocity magnitudes for the zero-heat-capacity argon added to air. It is obvious that this species does decreases the strength of the flame, but that its effect is much smaller than for the argon results shown in Figure 10. Based on an extinguishment temperature of 1550 K, the extinguishing concentration can be estimated as 73% or roughly 1.7 times greater than required for argon. This corresponds to an oxygen concentration of 5.7% at the LOI. Interestingly, the dependence of the maximum flame temperature at extinction on the fuel and oxidizer velocities is very similar for both sets of calculations as can be seen in Figure 20 where they are compared. The solid line is that shown in Figure 17, which was derived by fitting to the results for N_2, Ar, He, and CO_2. The data for the zero-heat-capacity argon fall slightly below those for argon, but it is clear that simple dilution of air has a similar effect on the flame as heat absorption by an inert. Assuming that the effects of heating an inert and dilution are additive, as suggested by this close correspondence, the effectiveness of Ar as a thermal agent is estimated to be 41% due to dilution and 59% due to heat extraction.

The availability of detailed flame structure information from the calculations allows the effect of a zero-heat-capacity diluent to be understood. As a starting point, it is important to recognize that flames burning in air and air diluted with a zero-heat-capacity agent have identical adiabatic flame temperatures. This suggests that the observed decreases in maximum temperature must be due to redistribution of the heat generated by combustion over a larger region of space and/or a reduction in the amount of heat released. In order to investigate this point, results for a methane counterflow diffusion flame burning in air are compared with those for a flame burning air diluted with 60% of the zero-heat capacity diluent in Figure 21. It is evident that while the maximum flame temperature is significantly reduced by the addition of the agent, the spatial temperature distributions are very similar for the two flames. This suggests that the primary effect of dilution is to reduce the amount of heat released.

Figure 22 shows CH_4 and O_2 mole fractions as a function of distance from the burner on a semi-log plot for both flames. It can be seen that while the primary fuel is completely reacted at the flame surface, some O_2 "leaks" from the oxidizer side to the fuel side. O_2 reaching the fuel side of the reaction layer eventually diffuses to a location where the temperature is low enough that reaction can no longer occur. At this point the O_2 acts like a diluent having a heat capacity with the result that the maximum temperature in the flame zone is reduced. Close inspection of Figure 22 shows that a significantly larger fraction of the available O_2 leaks through to the fuel side of the flame when the oxidizer is diluted air as opposed to air. This difference explains the lower maximum flame temperatures calculated for burning in air diluted by an agent having no heat capacity.

The leakage of O_2 through the flame front is due to the finite rates of reaction for oxidation reactions. Liñán and Williams provide a good introductory discussion of this behavior and the reasons for it. [80] Oxygen leakage was observed experimentally several decades ago [81] and was predicted by early calculations of counterflow diffusion flames [35]. Du and Axelbaum discuss the effect of O_2 leakage with respect to a series of methane flame where they systematically varied the stoichiometric mixture fraction while maintaining a constant adiabatic flame temperature. [70] These authors found that the flame strength increased with increasing stoichiometric mixture fraction and argued that this was due to the shift of the O_2 profile into regions of higher temperature. Decreased O_2 flame leakage was also evident in the calculations with higher stoichiometric mixture fraction. Lentati and Chelliah have also noted the importance of oxygen leakage for understanding flame extinction. [59] The increased O_2 leakage and decreased maximum flame temperature

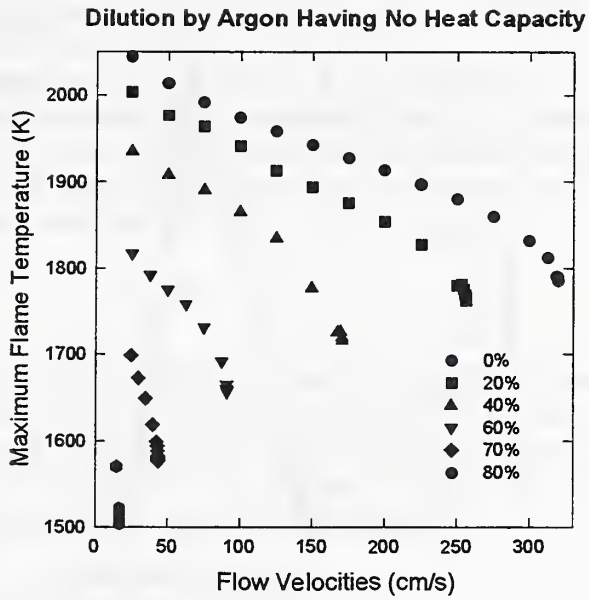

Figure 19. Maximum calculated flame temperatures are plotted against methane and oxidizer exit velocity magnitudes for a series of methane/air opposed flow diffusion flames diluted with a surrogate agent similar to argon, but with $C_p = 0$. Symbols correspond to the percentage of surrogate agent added.

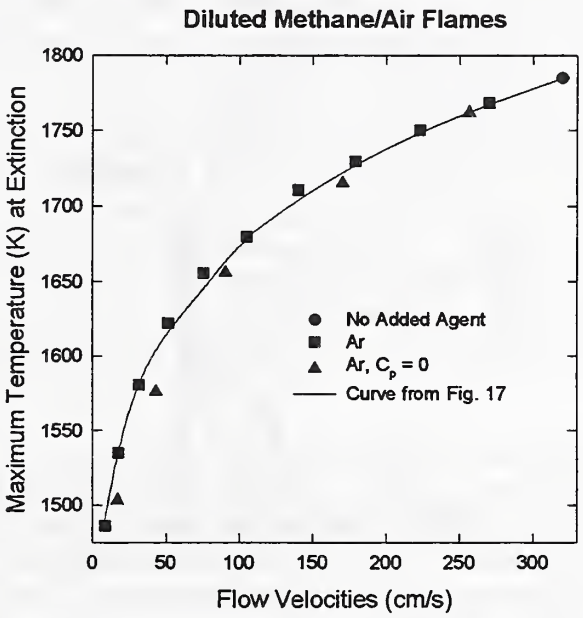

Figure 20. Values of maximum flame temperature at extinction are plotted as a function of fuel and oxidizer extinction velocity magnitudes for a range of concentrations of argon and a similar surrogate agent having $C_p = 0$. The solid line is the result of the regression fits shown in Figure 17.

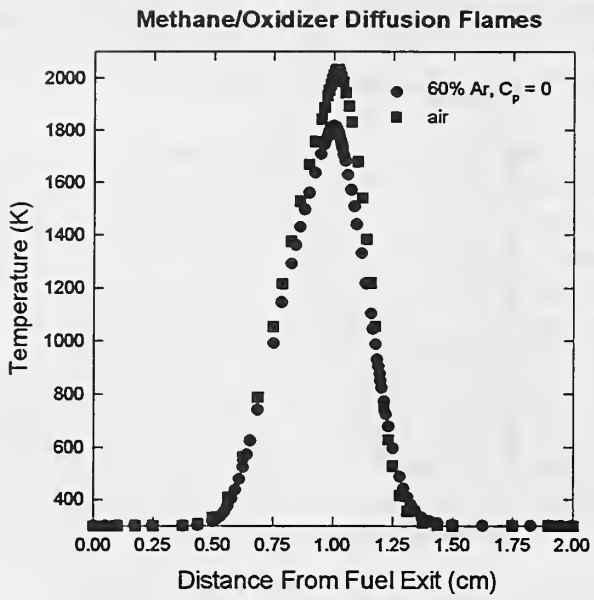

Figure 21. Temperature is plotted as a function of distance from the fuel exit for methane flames burning in air and air mixed with 60% of a diluent having similar properties to Ar, but with zero heat capacity. Fuel and air exit velocity magnitudes are 25 cm/s for both flames.

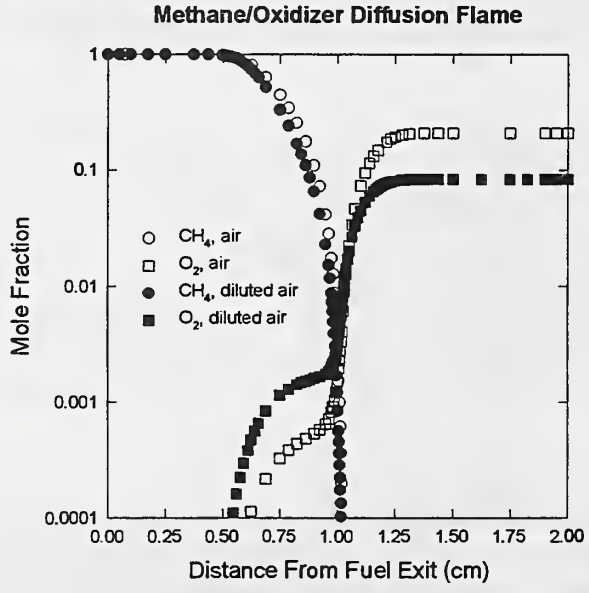

Figure 22. Calculated methane and oxygen mole fractions are shown on a semi-log plot as a function of distance from the fuel exit for methane flames burning in air (open symbols) and air mixed with 60% of a diluent having similar properties to Ar, but with zero heat capacity. Fuel and air exit velocity magnitudes are 25 cm/s for both flames.

observed with decreasing stoichiometric mixture fraction found for the current calculations are consistent with these trends.

One of the goals of the current work was to test the hypothesis that the effectiveness of a thermal agent depends on the location, relative to the high temperature flame zone, where heat extraction occurs. A surrogate thermal agent, X, was used for these calculations. The molecular weight, thermodynamic properties, and transport properties of X are identical to those of argon, but it is capable of undergoing a simple reaction with ambient gases to generate a new species, Y, i.e.,

$$X + M \rightarrow Y + M \quad . \qquad (14)$$

Y is also very similar to argon, the only difference being that its heat of formation is assigned an arbitrary positive value instead of being zero. As a result, when Reaction (14) takes place it extracts heat and cools the local surroundings by an amount equal to the heat of reaction, $\Delta H_{X\text{-}Y}$. Since X and Y do not react with any other species, the reaction is effectively simply a heat sink, and X therefore meets the definition of a thermal agent.

The rate constant for Reaction (14) is expressed as

$$k_{X \rightarrow Y} = A T^{\beta} e^{-E_a/RT} \quad , \qquad (15)$$

where A is the pre-exponential factor, β is the temperature exponent, E_a is the energy of activation, R is the gas constant, and T is temperature. By varying the parameters A, β, and E_a it is possible to change the temperature range over which the reaction occurs and hence the location relative to the flame zone for heat extraction. For the calculations which follow, initial values were chosen for A and β, and only the value of E_a was changed in order to vary $k_{X\text{-}Y}$. One problem faced in such calculations is that due to the variations in the residence time, which depends on the velocities of the fuel and oxidizer, the completeness of reaction over a given temperature range can vary with initial conditions. For this reason, a set of calculations was performed for one value of fuel and oxidizer exit velocity magnitudes in which E_a was varied. A relatively low value of 25 cm/s was chosen because this condition is close to that for which flame extinguishment occurs. An initial calculation was run for which the parameters in Eq. (15) were set to $A = 1\times10^{10}$ cm^3/(mole-s), $\beta = 0$, and $E_a =$ 25.1 kJ/mole, and the heat of formation for Y was chosen to be 96.1 kJ/mole. The concentration of X added to the air was 5%. Figure 23 compares the resulting temperature profile across the flame with that calculated for the case when 5% argon is added. The heat extracted by agent X has lowered the temperature on the oxidizer side below ambient. The maximum flame temperature with X is reduced, and its position has been shifted towards the oxidizer side relative to the case with argon.

It is clear from Figure 23 that the majority of the heat extraction is occurring at low temperatures for $E_a =$ 25.1 kJ/mole. This can seen in Figure 24 which shows X and Y mole fractions plotted as a function of distance from the fuel exit. The corresponding temperature profile is included as the solid line. The conversion of X to Y is well advanced before the boundary layer is reached at roughly 1.3 cm from the fuel exit, and then rapidly accelerates. The concentration of X has become nearly zero by the time the location on the oxidizer side is reached where the temperature has increased to 1200 K. The maximum calculated temperature for this flame is 1928 K, which can be compared with a value of 2006 K when 5% argon is used as the diluent.

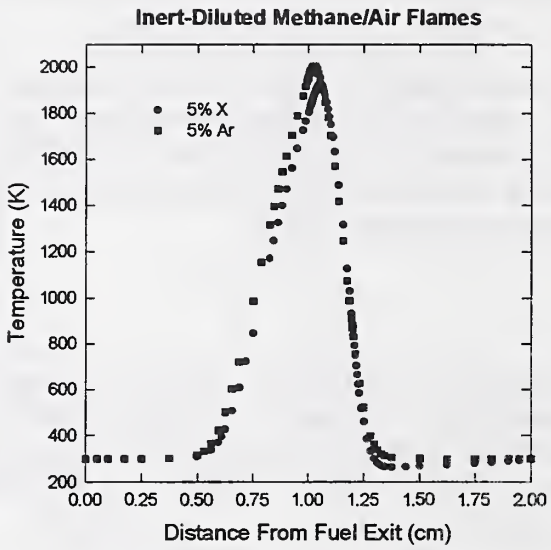

Figure 23. Calculated flame temperature is plotted as a function of distance from the fuel exit for methane/air diffusion flames where the oxidizer is diluted with 5% of either argon or the hypothetical agent X which reacts to form Y with E_a = 25.1 kJ/mole and ΔH_{X-Y} = 96.1 kJ/mole. Methane and oxidizer exit velocity magnitudes are 25 cm/s.

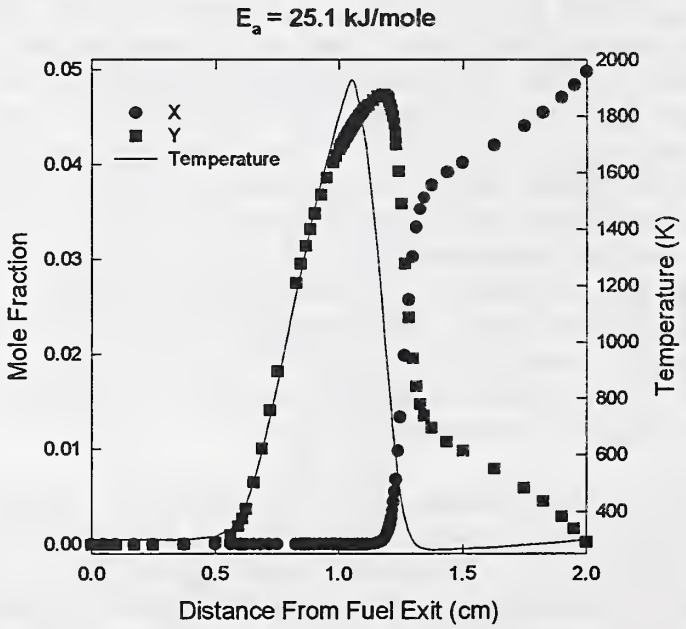

Figure 24. The mole fractions of X and Y are plotted as a function of distance from the fuel exit for a methane flame burning in air with 5% added X. X reacts to form Y with E_a = 25.1 kJ/mole and ΔH_{X-Y} = 96.1 kJ/mole. The spatial variation of temperature is also shown as the solid line. Methane and oxidizer exit velocity magnitudes are 25 cm/s.

In order to change the location where heat extraction takes place, the calculation was repeated for a series of increasing E_a. Figure 25 is similar to Figure 24, but is for the case with E_a increased to 58.6 kJ/mole. The reaction behavior of X is very different than observed for the lower E_a. The concentration of X does not decrease appreciably until the temperature begins to increase at the boundary layer. As the temperature begins to rise on the oxidizer side, conversion of X to Y begins and accelerates with increasing temperature. A substantial fraction of the conversion takes place for temperatures greater than 1600 K, but, even so, the amount of unreacted X reaching the rich side of the flame is minimal. A maximum temperature of 1934 K is calculated. This is very close to the value found for $E_a = 25.1$ kJ/mole.

Figure 26 shows the results when the E_a is increased to 83.7 kJ/mole. For this large energy of activation, the conversion of X to Y has become so slow that a substantial fraction of X passes through the high temperature zone without conversion to Y. As the temperature falls on the rich side of the flame, the reaction slows down, and the remaining X becomes kinetically "frozen" and simply diffuses toward the fuel side. As a result, the amount of heat absorption is less than that occurring when X fully reacts. This is reflected in the maximum calculated flame temperature of 1963 K, which is intermediate between that found for X with lower E_a's and that for 5% argon, which only has dilution and heat capacity effects.

Figure 27 shows the maximum calculated flame temperature as a function of assumed E_a for a series of calculations carried out for 5% X added to the air. For $E_a \leq 50$ kJ/mole the calculated temperature is constant within the variations expected for the different grids used for the calculations. As the E_a is increased further, the maximum temperature begins to increase. As we have seen, this is due to some fraction of X passing through the flame to the rich side without reacting to form Y. Since the temperature range over which the heat is absorbed by the reaction of X to Y varies widely as the E_a increases from 25 kJ/mole to 50 kJ/mole, these findings show that the maximum flame temperature and, by extension, flame extinction only depend on the amount of heat extracted and not where it occurs relative to the flame zone. It is concluded that the original hypothesis concerning the role of heat absorption location by gaseous thermal agents on extinguishment is not valid. This conclusion should be contrasted with the recent results of Lentati and Chelliah, who report that the location where heat extraction occurs can be important for flame inhibition when evaporating water droplets are added to the oxidizer flow. [58,59] Their finding seems to be associated with the fact that larger water droplets do not follow the oxidizer flow streamlines, whereas gaseous agents do.

A complete set of calculations was carried out for species X having $\Delta H_{X\text{-}Y} = 96.1$ kJ/mole and $E_a = 41.8$ kJ/mole. The results are plotted in Figure 28 as maximum calculated flame temperature versus exit velocity magnitudes for methane and oxidizer. Based on an extinction temperature of 1550 K, the extinguishing concentration for X in air is estimated to be 15.9%. The corresponding value for argon was 43%. Thus the heat extracted by the reaction of X to Y has reduced the amount of agent required by nearly 2/3. Figure 29 compares calculated values of maximum flame temperature as a function of velocity for 15%, 30%, and 45% added argon with the corresponding results for 5%, 10%, and 15% X. The two set of curves fall close together, but the agreement is not complete. At the lower concentrations the results for X fall slightly below those for Ar, while the opposite is true for the highest concentrations. This behavior is most likely associated with the nonlinear dependence of the maximum flame temperature on concentration evident in Figure 18 and the contribution of dilution to extinguishment.

The effect of doubling the amount of heat absorbed by X was considered by running a series of calculations for $\Delta H_{X\text{-}Y} = 192.1$ kJ/mole. Calculated maximum flame temperatures are plotted as a function of the exit velocity magnitudes for methane and oxidizer in Figure 30. From these results the extinction concentration for X with the higher heat absorption can be estimated as 9.7%. This value is roughly 60% of that found with $\Delta H_{X\text{-}Y} = 95.2$ kJ/mole, or 20% higher than would be expected if flame extinguishment was due solely to the heat extracted. The most likely source for the difference is the effect of dilution discussed earlier. The

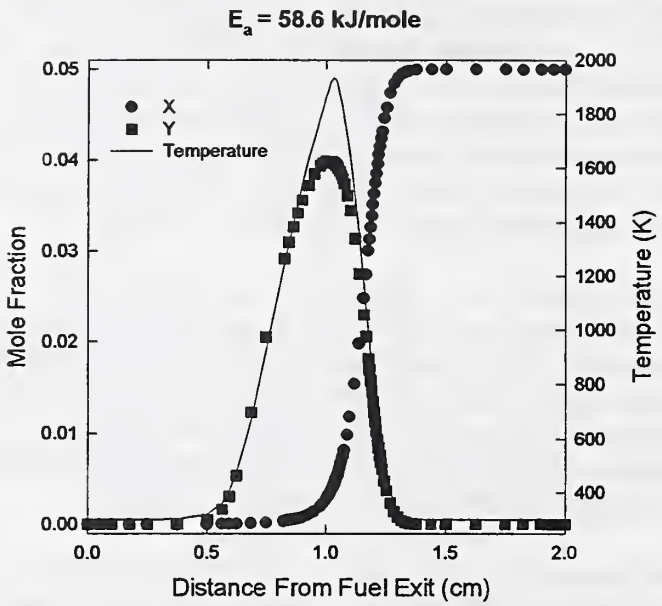

Figure 25. The mole fractions of X and Y are plotted as a function of distance from the fuel exit for a methane flame burning in air with 5% added X. X reacts to form Y with E_a = 58.6 kJ/mole and ΔH_{X-Y} = 96.1 kJ/mole. The spatial variation of temperature is also shown as the solid line. Methane and oxidizer exit velocity magnitudes are 25 cm/s.

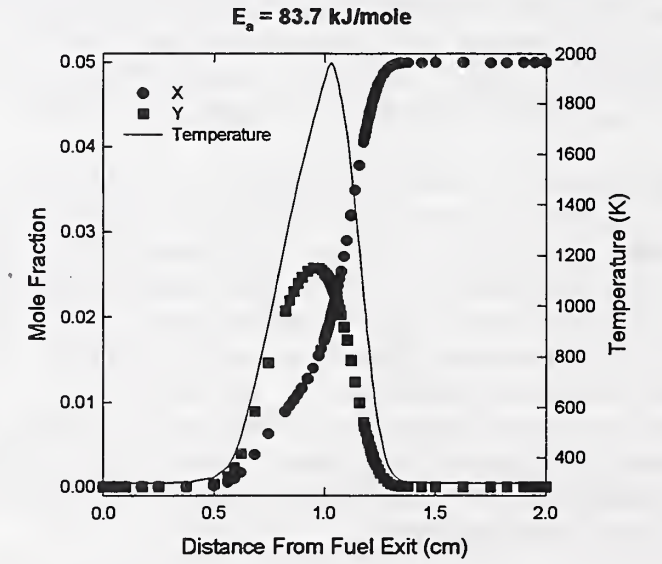

Figure 26. The mole fractions of X and Y are plotted as a function of distance from the fuel exit for a methane flame burning in air with 5% added X. X reacts to form Y with E_a = 83.7 kJ/mole and ΔH_{X-Y} = 96.1 kJ/mole. The spatial variation of temperature is also shown as the solid line. Methane and oxidizer exit velocity magnitudes are 25 cm/s.

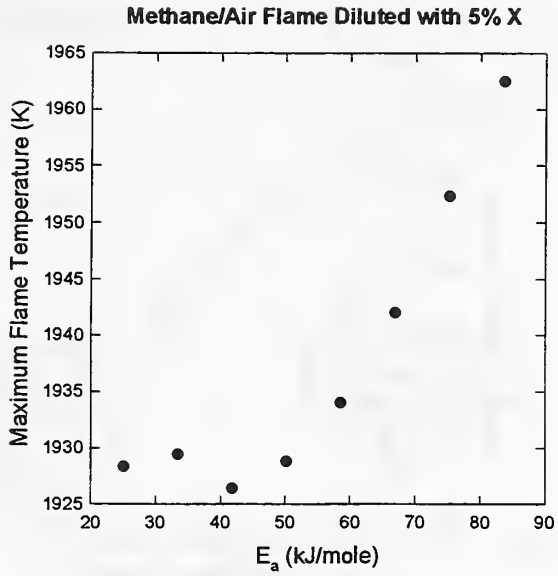

Figure 27. Values of maximum flame temperature for methane flames burning in air diluted with 5% X are plotted as a function of the energy of activation for the conversion of X to Y. Methane and oxidizer exit velocity magnitudes are 25 cm/s.

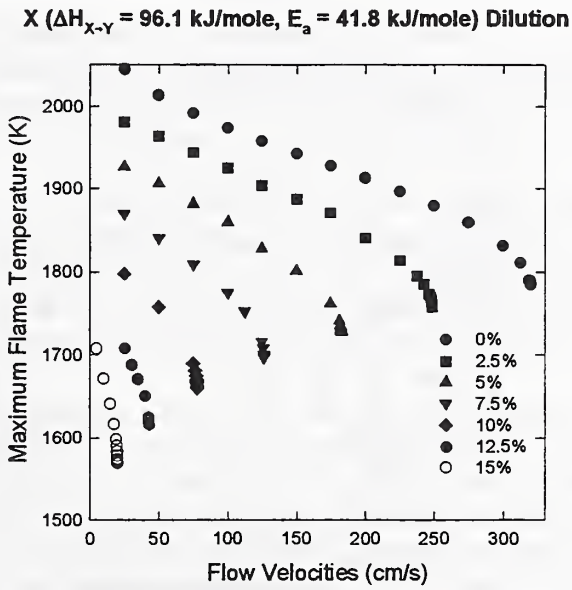

Figure 28. Maximum calculated flame temperatures are plotted against methane and oxidizer exit velocity magnitudes for a series of methane/air opposed flow diffusion flames diluted with agent X which reacts to form Y with E_a = 41.8 kJ/mole and ΔH_{X-Y} = 96.1 kJ/mole. Symbols correspond to the percentage of added X.

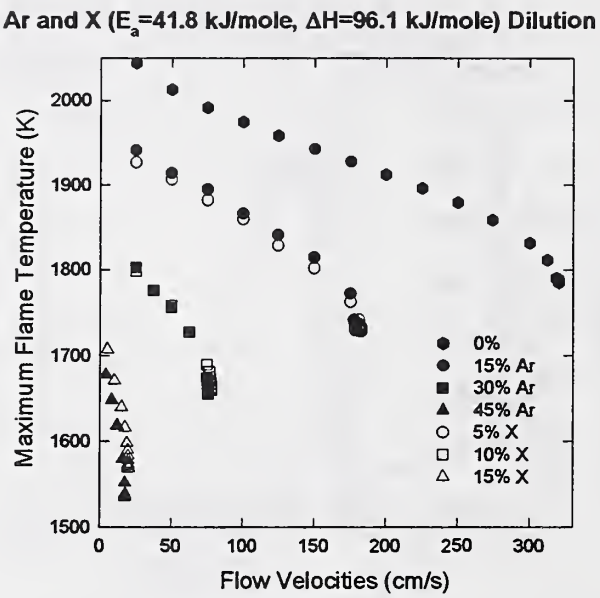

Figure 29. Maximum calculated flame temperatures are plotted against methane and oxidizer exit flow velocity magnitudes for a series of methane/air opposed flow diffusion flames diluted with argon and agent X (E_a = 41.8 kJ/mole and ΔH_{X-Y} = 96.1 kJ/mole).

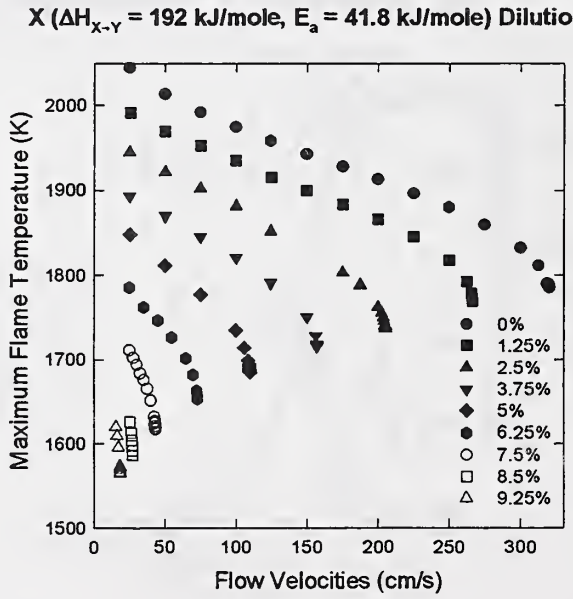

Figure 30. Maximum calculated flame temperatures are plotted against methane and oxidizer exit flow velocity magnitudes for a series of methane/air opposed flow diffusion flames diluted with agent X which reacts to form Y with E_a = 41.8 kJ/mole and ΔH_{X-Y} = 192.1 kJ/mole. Symbols correspond to the percentage of added X.

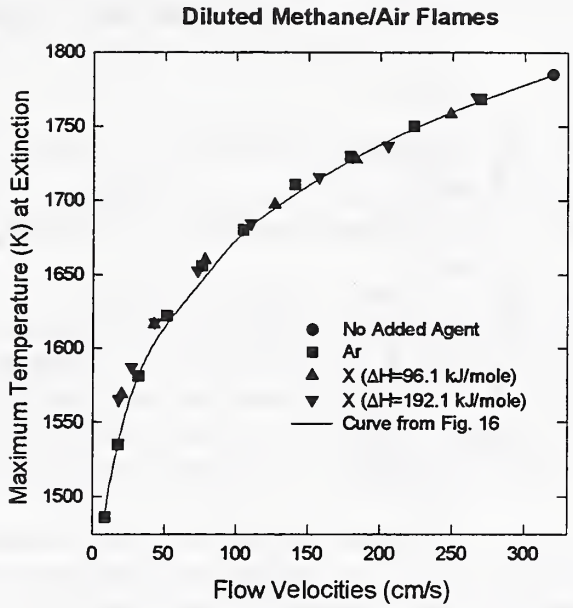

Figure 31. Values of maximum flame temperature at extinction are plotted as a function of fuel and oxidizer exit velocity magnitudes for air diluted with a range of concentrations of argon and surrogate agent X having ΔH_{X-Y} = 96.1 kJ/mole or 192.1 kJ/mole. The solid line is the result of the regression fits shown in Figure 17.

concentration of added agent required for flame extinguishment decreases as the amount of heat it can absorb increases, but the decreased concentration reduces the degree of dilution, with the result that the effectiveness of extracting additional heat is offset somewhat.

The role of dilution has an important implication with regard to simple estimates of extinguishing efficiency for thermal agents which are often obtained by taking ratios of heat capacities for various agents. If the agents have a large heat capacity difference, and the percentages required for extinguishment therefore differ substantially, a simple linear dependence on heat capacity should not be observed. In fact, the agent having the largest heat capacity should be less effective than expected, as observed in the current calculations.

Figure 31 shows a plot of maximum flame temperature at extinction versus exit flow velocity magnitudes for air diluted with various concentrations of argon and X with ΔH_{X-Y} = 96.1 kJ/mole and 192.1 kJ/mole. The solid line is the result shown in Figure 17 based on a fit to data for known thermal agents. Despite the fact that the amount of agent required for extinction varies nonlinearly with ΔH_{X-Y}, the data all fall very close together. This supports the conclusion that assuming a common extinction temperature should provide excellent estimates for flame extinguishing concentrations of thermal agents. The slight variations present near the extinguishing concentration are likely due to dilution effects.

G. Prediction of Extinguishing Concentration for HFE7100

The first section of this report summarizes data base searches which yielded a list of thermal agents which are expected to be particularly effective. In order to obtain some idea of the concentrations which might be

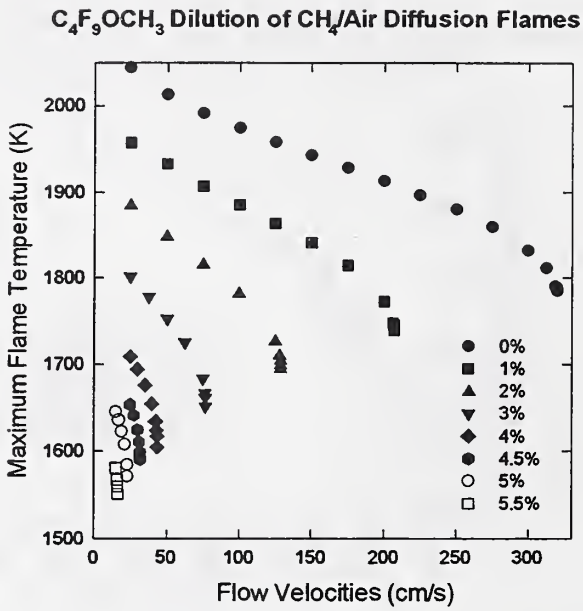

Figure 32. Maximum calculated flame temperatures are plotted against methane and oxidizer exit velocity magnitudes for a series of methane/air opposed flow diffusion flames diluted with $C_4F_9OCH_3$. Symbols correspond to the percentage of added $C_4F_9OCH_3$.

required for extinguishment by such agents, a series of calculations were carried out for a compound which is predicted to be one of the more effective, methoxy-nonafluorobutane ($C_4F_9OCH_3$; HFE7100). It was assumed that the only mechanism for heat extraction was the heat capacity of the gaseous agent, even though significant heat could also be removed by evaporation if the agent were released as a liquid at room temperature. It is also true that this molecule is likely to decompose as it enters the high temperature region of the flame and will react to form final products. Reaction of the agent was not modeled. Due to the presence of a large number of fluorine atoms, it is also likely that the extinguishing efficiency will include a small chemical component. [33,52,53,54] On this basis it might be expected that the result of this calculation will be an upper limit for the required extinguishing concentration.

Figure 32 shows maximum flame temperature as a function of the methane and oxidizer exit velocity magnitudes. As now expected, the curves have similar appearances to those found for the other thermal agents. However, what is particularly noteworthy is the relatively small mole fraction of $C_4F_9OCH_3$ required to lower the maximum flame temperature to the extinguishment temperature of 1550 K. The addition of only 5.5% of $C_4F_9OCH_3$ is calculated to be sufficient. The high heat capacity of this molecule due to its large number of atoms makes it a particularly effective thermal agent in molar terms. If liquid vaporization and chemical effects improve its effectiveness still further, this species may well approach the effectiveness of halon 1301, which has an extinguishing concentration of 2.9% [78] on a molar basis. On a mass basis this fluorinated ether will be less effective, based on the molecular weights of 148.9 g/mole for halon 1301 and 250 g/mole for $C_4F_9OCH_3$, but not dramatically so. It might be expected that the mass fraction of $C_4F_9OCH_3$ which must be added would be similar to other agents which do not have a strong component of chemical effectiveness. [76]

The vapor pressure for $C_4F_9OCH_3$ as a function of temperature is given by [16]

$$P_{C_4F_9OCH_3} = e^{10.839-\frac{3627.2}{T}}, \qquad (16)$$

where $P_{C_4F_9OCH_3}$ is the partial pressure of $C_4F_9OCH_3$ in atmospheres and T is the temperature in K. For 300 K and atmospheric pressure the saturation percentage of the ether in air is calculated to be 29%. Thus the saturation pressure at room temperature should be more than sufficient to extinguish a diffusion flame.

Two experimental measurements of the concentration of methoxy-nonafluorobutane required to extinguish diffusion flames have been identified. Unpublished measurements from the New Mexico Engineering Institute using a standard cup burner with heptane fuel yielded an extinguishing concentration of 6.1 volume per cent. [82] In a patent disclosure, Flynn and Scott also reported that a value of 6.1 volume per cent was sufficient to extinguish a butane flame in a "micro-cup burner". [83] These values are 11% higher than estimated using detailed chemical kinetic modeling for the extinguishment of a methane flame.

Earlier it was shown that cup burner measurements using heptane fuel for agents known to act only thermally yielded extinguishing concentrations which were roughly 90% - 95% of those estimated using detailed kinetic modeling. This would suggest that the expected difference between calculated and experimental values for $C_4F_9OCH_3$ are actually somewhat greater than indicated above. A plausible explanation for this difference is the effect of chemical reactions. If this is the indeed the case, the results indicate that the net effect of reactions involving this agent is to decrease its effectiveness slightly from that expected if it acted simply as a nonreactive thermal agent. Other reaction effects must counteract the expected small chemical enhancement due to the fluorine atoms.

H. Discussion and Summary

Detailed chemical kinetic modeling of counterflow diffusion flames has been shown to be an effective approach for improving the understanding of the effects of thermal agents and for predicting flame extinction and extinguishment behaviors. Important findings of the study are summarized here.

Exit flow velocities, the various strain rates, and the stoichiometric scalar dissipation rate calculated for extinction of a given flame are strongly dependent on the detailed chemical kinetic mechanism used. The mechanism employed here, GRI-Mech 1.2, predicts flames which are more robust than observed experimentally. On the other hand, the maximum flame temperatures for flames at extinction seem to be relatively independent of mechanism. This is relevant for the current work because a particular maximum flame temperature at extinction is used as the criteria for flame extinguishment.

Flame radiation is expected to have a noticeable effect on flame structure for the conditions relevant to extinguishment of diffusion flames. Recent detailed modeling investigations which incorporate radiation indicate that the relative importance of radiation increases with decreasing strain rate. For the strain rates typical of extinguishment of buoyancy-dominated diffusion flames, the effects of radiation represent a relatively small fraction of the total heat release. The neglect of radiation does not appear to seriously limit predictions of extinguishing concentrations, even though its neglect would be expected to change such properties as the extinguishing limit temperature and strain rate.

Assuming a maximum flame temperature at extinction of 1550 K for extinguishing conditions provides good agreement between the experimental result and the model prediction of the extinguishing concentration for

nitrogen added to the air side for laminar methane/air diffusion flames. Similarly, the calculated extinguishing concentration for Ar added to Ar "air" agrees well. Even though experimental data for extinguishment of methane/air flames is lacking for other thermal agents, comparisons of extinguishing concentration predictions for Ar, CO_2, and He added to air agree closely with values for cup burners fueled with heptane. The strain rates which generate this extinguishment temperature depend very weakly on agent. For all cases the strain rates are on the order of a few tens of inverse seconds.

Surrogate thermal agents having unrealistic physical behaviors have been used to computationally investigate particular aspects of flame extinguishment. Use of an agent having no heat capacity has shown that dilution effects can weaken and ultimately extinguish diffusion flames due to an increase in the amount of oxygen leaking through the flame front. An agent X which is capable of reacting to form Y while extracting a well characterized amount of heat was used to demonstrate that the effectiveness of a thermal agent is insensitive to the location where heat extraction occurs relative to the flame front for steady flames as long as the cooled gases are ultimately convected into the flame zone. By varying the heat absorbed by a given amount of X, it was shown that there is not a one-to-one correspondence between the amount of heat extracted by an agent and the concentration required for flame extinguishment. This observation was attributed to the role of dilution on extinguishment.

The extinguishing concentration of methoxy-nonafluorobutane for methane flames was estimated as 5.5 mole per cent using the approach developed during the current investigation. It was assumed that this species acts simply as a thermal agent. Experimental values for heptane- and butane-fueled diffusion flames were roughly 11% larger. The small difference between prediction and experiment was attributed to the decomposition and subsequent reaction of this agent in the flame, i.e., to chemistry effects.

IV. SURFACE COOLING

A. Introduction

When liquid suppressant droplets released from a discharge port approach a fire, several things can happen. Droplets with sufficient momentum to penetrate the flame, depending on their sizes, can either be consumed in the flame (participate directly in the suppression processes through physical and/or chemical mechanisms) or reach the fuel surface. Droplets with little momentum (*e.g.*, very small droplets) may not penetrate the fire and will be deflected away by the rising hot plume. [84] These deflected droplets will eventually evaporate or strike adjacent objects. For droplets landing outside the burning area, the cooling of the adjacent and surrounding surfaces could mitigate or contain the flame spread processes. Therefore, droplet interaction with surfaces is an integral part in the understanding of the overall suppression processes.

One of the possible fire suppression mechanisms using a liquid fire suppressant (*e.g.*, water) is fuel surface cooling. The relatively cool impacting droplets will interact with the relatively hot fuel surface. One of the droplet/surface interactions is the extraction of heat from the surface to vaporize the continuously deposited droplets, thereby reducing the surface temperature. The burning rate falls, which leads to a decrease in heat feedback to the fuel surface. Eventually, a critical burning rate is reached beyond which combustion can no longer be sustained. The other effect of the deposited droplets on the burning rate is the reduction of mass transfer area on the fuel surface, which also causes a reduction in burning rate.

In order to understand surface cooling without resorting to a detailed analysis of the coupling between the transient thermal response of the fuel bed as a result of the application of liquid agent and the heat feedback

from the flame to the fuel, the transient coupling process is considered as a series of quasi-steady steps. At any instant in time, a steady-state energy balance at the fuel surface can be written as:

$$\dot{m}''_{fuel}\,\Delta H_{fuel} = Q''_{cond} + Q''_{conv} + \varepsilon_{flame}\,\sigma\,T^4_{flame} - \varepsilon_s\,\sigma\,T^4_{surf} - q'' \qquad (17)$$

where $\dot{m}''_{fuel}$ is the fuel burning mass flux, ΔH_{fuel} is the effective heat of gasification of the fuel, Q''_{cond} is the conductive heat flux to the fuel surface, Q''_{conv} is the convective heat flux to the fuel surface, ε_{flame} is the flame emissivity, σ is the Stefan-Boltzmann constant, T_{flame} is the average flame temperature, ϵ_s is the surface emissivity, T_{surf} is the fuel surface temperature, and q'' is the heat flux removal from the fuel surface due to surface cooling.

The surface cooling heat flux, q'', depends on the interaction of the liquid droplets with the surface. There are many different scenarios of droplet impact on a surface. The impacting processes depend on the thermophyscial and geometrical properties of the drop and of the target surface and on the magnitude and direction of the impact velocity vector. In addition, for a flaming surface, the droplet will traverse through an environment different from that of a non-burning surface before impact. However, in the literature, droplet/surface interaction studies focus almost exclusively on non-burning surfaces.

When relatively cool liquid droplets impact on a solid surface, cooling of the surface occurs as a result of heat transfer between the surface and the droplets. A liquid droplet impacting a solid surface has been extensively studied in the literature. [85,86,87,88,89,90,91,92,93] Maps which identify the various impact and heat transfer regimes over a wide range of experimental conditions have been constructed. Spray cooling or quenching of hot metallic surfaces has also been extensively studied. [94,95,96,97,98,99] Many empirical heat transfer correlations for spray cooling applications exist.

For a liquid droplet interaction with a *liquid* surface, several scenarios need to be considered, and the impact dynamics are complicated by the ability of the liquid surface to deform and to displace in response to the impinging droplet and by the internal fluid motion of the liquid pool initiated by the impact processes. [100] If the droplet has a very high impact velocity, it can cause a crater in the liquid pool and a splash upon impact. For a burning liquid pool, the splash may result in a sudden increase in burning rate due to an increase in the liquid surface area caused by the splash droplets. If the droplet is soluble in the liquid, mass transfer between the penetrating droplet and the liquid will occur. Depending on droplet impact parameters, differences in miscibilities and physical properties (surface tension and viscosity) between the droplet and the target liquid, and the depth of the liquid layer, the droplet may float on the surface, may coalesce into the liquid pool with little or no splashing and produce a vortex ring, may rebound or splash, forming a crater and a small jet or column of liquid at the surface, or may dissolve into the liquid pool. Most work in the literature has examined the isothermal impact of a liquid droplet onto a surface of the same liquid (e.g., see the review article of Rein [100] and the references therein). In a fire suppression scenario, the impacting droplet encounters a different liquid target (suppression fluid versus fuel) with different physical properties. The temperature of the droplet can be much lower than that of the liquid surface (especially, in the case of burning), and the contact between a cold droplet with a hot liquid may sometimes results in vapor explosion [101], an unwanted situation. All of these complicated factors render the study of heat transfer processes between liquid droplets and a liquid surface an arduous and daunting task. To the best of our knowledge, appropriate heat transfer correlations do not exist in the literature; therefore, liquid surface cooling calculations, in spite of the importance of the process, will not be attempted here.

In this section, we will discuss droplet evaporation and solid surface cooling by droplets. Droplet evaporation is considered because it is an integral part of the surface cooling problem. If the droplets evaporate completely before reaching the fuel surface, the heat removal from the surface will decrease significantly due to the fact that the liquid latent heat of vaporization does not play a role. Under this circumstance, the surface will only be cooled by a vapor jet, which is not an effective cooling mechanism.

Another important aspect in surface cooling is the ability of the droplets to reduce the surface temperature of metallic components in the vicinity of a fire to prevent re-ignition, which is a potential problem in suppressing aircraft engine nacelle fires. If sufficient cooling of hot surfaces cannot be achieved after the release of fire suppressant, re-ignition of residual fuel vapor/air mixture by hot surfaces may occur.

In the following discussion, the five fluids (water, lactic acid, $C_3F_5H_3O$, HFE7100, and R338mccq) identified in Section II as having the highest ΔH^{total} (mass basis) are considered to evaluate their droplet vaporization and surface cooling characteristics. Low boiling-point fluids will not be considered here because under typical operating conditions, these fluids can be easily flash-vaporized soon after they leave the discharge opening; thus they likely arrive at the surface in the form of a vapor.

B. Evaporation of Liquid Droplets

The estimation of liquid droplet evaporation is based on the classical d^2-law, which gives the droplet diameter as a function of time as

$$D^2 = D_o^2 - Kt \quad , \tag{18}$$

where D is the instantaneous droplet diameter, D_o is the initial droplet diameter, t is the time, and K is the evaporation constant. The evaporation constant can be calculated by

$$K = \frac{8 k_g \ln(1+B)}{\rho_F C_{pg}} \quad , \tag{19}$$

where B is the transfer number, k_g is the gas-phase thermal conductivity, C_{pg} is the gas-phase heat capacity, and ρ_F is the liquid density. The B number based on mass transfer considerations is given by

$$B_M = \frac{Y_{FS} - Y_{F\infty}}{1 - Y_{FS}} \quad , \tag{20}$$

where Y_{FS} and $Y_{F\infty}$ are the vapor-phase mass fraction at the droplet surface and ambiance, respectively. The mass fraction, Y_{FS}, can be evaluated by

$$Y_{FS} = \frac{P_{FS} M_F}{P_{FS} M_F + (P - P_{FS}) M_A} \quad , \tag{21}$$

where P_{FS} is the liquid vapor pressure at the droplet surface, P is the ambient pressure, which is equal to the sum of the liquid vapor pressure and partial pressure of air at the droplet surface, and M_F and M_A are the molecular weights of liquid and air, respectively.

The B number based on heat transfer considerations is given by

$$B_T = \frac{C_{pg}(T_\infty - T_s)}{\Delta H_{vap}} \quad , \qquad (22)$$

where T_∞, T_s, and ΔH_{vap} are the ambient temperature, droplet surface (wet-bulb) temperature, and latent heat of vaporization of the liquid, respectively. Under steady-state conditions, $B_M = B_T$, and either Eq. (20) or Eq. (22) may be used to calculate the evaporation constant in Eq. (19).

If T_s is known, the calculation of evaporation constant is straightforward; however, under normal circumstances it is necessary to determine T_s in order to evaluate B and K. The calculation procedure can be found in references [102,103,104]. The basic idea is to find T_s such that $B_M = B_T$. Spalding [102] and Kanury [103] used a graphical approach. By plotting B_M and B_T against T_s, the intersection of these two curves defines the wet-bulb temperature and the corresponding B. An iterative method was used by Chin and Lefebvre. [104] The calculations presented here use the latter approach.

To calculate K, the reference temperature and mass fractions (based on the one-third rule [104]) were used to estimate the gas-phase thermophysical properties,

$$T_r = T_s + \frac{T_\infty - T_s}{3} \qquad (23)$$

$$Y_{Fr} = Y_{FS} + \frac{Y_{F\infty} - Y_{FS}}{3} \qquad (24)$$

$$Y_{Air} = 1 - Y_{Fr} \quad , \qquad (25)$$

where Y_{air} is the air mass fraction at the reference state. The equation for calculating the gas-phase heat capacity, C_{pg}, is given by

$$C_{pg}(T_r) = Y_{Air}\, C_{pA}(T_r) + Y_{Fr}\, C_{pF}(T_r) \qquad (26)$$

where C_{pA} is the heat capacity of air and C_{pF} is the gas-phase heat capacity of the fluid, all evaluated at T_r. The thermal conductivity of the gas phase is estimated by the following equation,

$$k_g(T_r) = Y_{Air}\, k_A(T_r) + Y_{Fr}\, k_F(T_r) \quad , \qquad (27)$$

where k_A is the thermal conductivity of air and k_F is the gas-phase thermal conductivity of the liquid, all evaluated at T_r.

The conditions used in the calculations were: (1) T_∞ = 1400 K (to simulate a flaming ambiance), (2) $Y_{F\infty} = 0$, and (3) P = 0.101 MPa.

The thermophysical properties of air, water, and lactic acid were obtained from the database of the Design Institute for Physical Properties. [1] The properties of $C_3F_5H_3O$, HFE7100, and R338mccq were estimated by methods described in Reid *et al.* [105]; the modified Rackett technique was used for ρ_F, the method of Joback for C_{pF}, the method of Lee and Kesler for P_{FS}, the method of Pitzer's acentric factor correlation for ΔH_{vap}, and the method of Ely and Hanley for k_F.

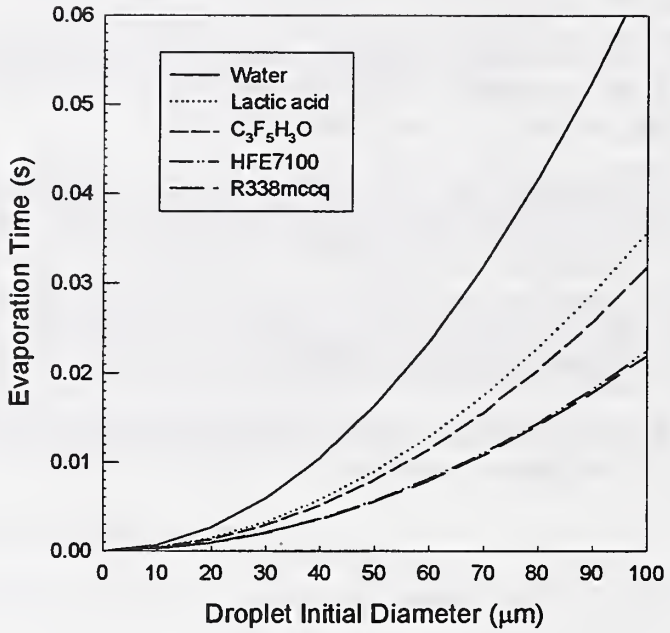

Figure 33. Droplet evaporation time as a function of initial droplet diameter.

Figure 33 shows droplet evaporation times, t_b, as a function of initial droplet diameter. The droplet evaporation time can be easily obtained by assigning $D = 0$ in Eq. (18) once K is known,

$$t_b = \frac{D_o^2}{K}. \qquad (28)$$

For a given initial droplet diameter under the same ambient conditions, the evaporation time for a water droplet is the longest and for a R338mccq droplet the shortest. For the five fluids examined, the ranking based on droplet evaporation times is

$$t_{b,R338mccq} < t_{b,HFE7100} < t_{b,C_3F_5H_3O} < t_{b,lactic\ acid} < t_{b,water}. \qquad (29)$$

How fast a droplet evaporates determines whether it will still remain as a droplet upon reaching the surface. However, if *flame cooling* is the dominant fire suppression mechanism, then it would be better to have the droplet completely vaporized in the flame.

C. Spray Cooling

In order to assess surface cooling, we consider the literature on spray cooling and quenching of hot metallic surfaces. The application of spray-cooling correlations to fuel surface cooling is only appropriate when the fuel surface is solid (*e.g.*, a PMMA or wood slab). Even in this case, care should be exercised because subtle differences in cooling mechanisms exist. A burning PMMA surface in reality is in a molten state, and wood forms a porous char layer. The interactions of droplets with molten and porous surfaces remain very difficult

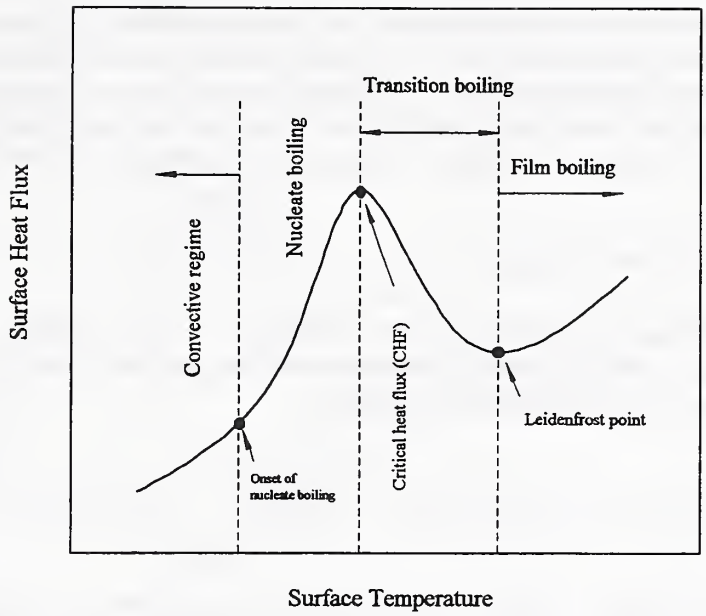

Figure 34. An illustration of a typical boiling curve associated with quenching of a hot surface.

problems to tackle. Differences also arise between fuel surface cooling and quenching of metallic surfaces. In the latter, radiation heat transfer to the droplets only comes from the heated surface; however, in the former, it also comes from the flame. Strictly speaking, the following calculations are more applicable to the cooling of a hot surface to prevent re-ignition than to the cooling of a burning fuel surface.

Depending on the surface temperature, when a hot surface is being quenched by a liquid spray, its surface will experience several distinct heat transfer regimes which can be followed along the "boiling curve". Such a curve is a plot of surface heat flux versus surface temperature and represents the strong relationship between heat flux and surface temperature during quenching. The characteristics of the boiling curve are classified as (with increasing surface temperature): (1) convective, (2) nucleate boiling, (3) critical heat flux, (4) transition boiling, (5) Leidenfrost point, and (6) film boiling. Detailed descriptions are available. [94,95] Figure 34 is an illustration of a boiling curve associated with spray cooling of a hot surface. The general features of the curve are similar to those for a pool boiling curve.

Since the boiling curve of one fluid may differ from that of other fluids, there are several important assumptions that have to be made in the following analysis.

When a comparison of surface heat fluxes is made, it is assumed that for the prevailing surface temperature, these fluids are in the *same* regime on the boiling curve. This assumption may not be valid because, for example, the surface temperatures at which the critical heat flux and Leidenfrost phenomena occur may be significantly different among the fluids studied; therefore, while one fluid may be at the critical heat flux, the other fluid may be in the nucleate boiling regime at the prevailing surface temperature. Unfortunately, in most cases, it is not possible *a priori* to determine the demarcation point (surface temperature) from one cooling regime to another without resorting to experimental observations.

The second assumption is that the dimensionless heat transfer correlations obtained in the literature using water (in most cases) are applicable to other fluids considered here. A third assumption is that the effect of surface roughness on surface heat flux is not considered. Furthermore, the spray parameters used in the

following calculations were chosen to be within the range of applicability of the empirical correlations. These operating parameters, though encountered in spray quenching applications, may not be identical to those appropriate for fire fighting applications. In addition, since different droplet generation techniques (sprays *vs.* mono-dispersed droplet streams) have been used to obtain the heat transfer correlations in various regimes, it is imperative that a comparison among the calculated surface heat fluxes should be made with these fluids in the *same* regime.

D. Convective Regime

Mudawar and co-workers [94,95] have performed extensive studies on cooling of metal surface in this regime using water sprays. Their heat transfer data were correlated using the Nusselt number, the Reynolds number, and the Prandtl number by the following expression,

$$\frac{h\,D_{32}}{k_f} = Nu = 2.512\left[\frac{Q''\,D_{32}}{\nu_f}\right]^{0.76}\left[\frac{C_{pf}\mu_f}{k_f}\right]^{0.56} = 2.512\,\mathrm{Re}^{0.76}\,\mathrm{Pr}^{0.56}, \qquad (30)$$

where h is the heat transfer coefficient, k_f is the thermal conductivity of the liquid, ν_f is the liquid kinematic viscosity, C_{pf} is the liquid heat capacity, and μ_f is the liquid viscosity. The Reynolds number is based on the volumetric spray flux, Q'', and the Sauter mean diameter, D_{32}, of the spray. All the liquid properties are evaluated at $(T_{surf} + T_f)/2$ where T_f is the droplet temperature before impact.

Figure 35 shows the calculated heat flux as a function of $T_{surf} - T_f$. The calculations were performed using Q'' = 0.005 m^3/m^2-s, T_f = 295 K, and D_{32} = 0.5 mm. The thermophysical properties of water and lactic acid were obtained from the DIPPR. [1] The properties of $C_3F_5H_3O$, HFE7100, and R338mccq were estimated by methods described in Reid *et al.* [105]; the boiling point method of Sato was used for k_f, the corresponding states method of Rowlinson for C_{pf}, and the method of Brule and Starling for μ_f. In this regime, water removes heat from the surface more efficiently than the other four fluids. It should be noted that it may not be feasible in practice to maintain the same D_{32} with a fixed Q'' (the conditions used in the calculations) for the five fluids because the atomization characteristics at the spray nozzle would be vastly different among the fluids owing to their thermophysical properties, thus resulting in different D_{32}. [106]

E. Nucleate Boiling Regime

Compared to other regimes on the boiling curve, the nucleate boiling regime in spray cooling is probably the least studied. In this regime, the heat flux removal from the surface was found to scale only with $T_{surf} - T_f$ in the studies by Mudawar and co-workers [94,95] where a water spray was used. The heat flux, q'', was correlated in the form of

$$q'' = 1.87\times10^{-5}\,(T_{surf} - T_f)^{5.55}. \qquad (31)$$

In the work of Qiao and Chandra [107] on nucleate boiling enhancement using a surfactant/water solution, the heat flux measurements could also be correlated well by scaling with $T_{surf} - T_f$ in a form similar to Eq. (31),

$$q'' = 0.56\times10^{-5}\,(T_{surf} - T_f)^{6}. \qquad (32)$$

If we *assume* that the proportionality constant and the power in the scaling law do not change significantly among the five chemical compounds and that the heat flux can be scaled with $(T_{surf} - T_f)$, then the heat flux

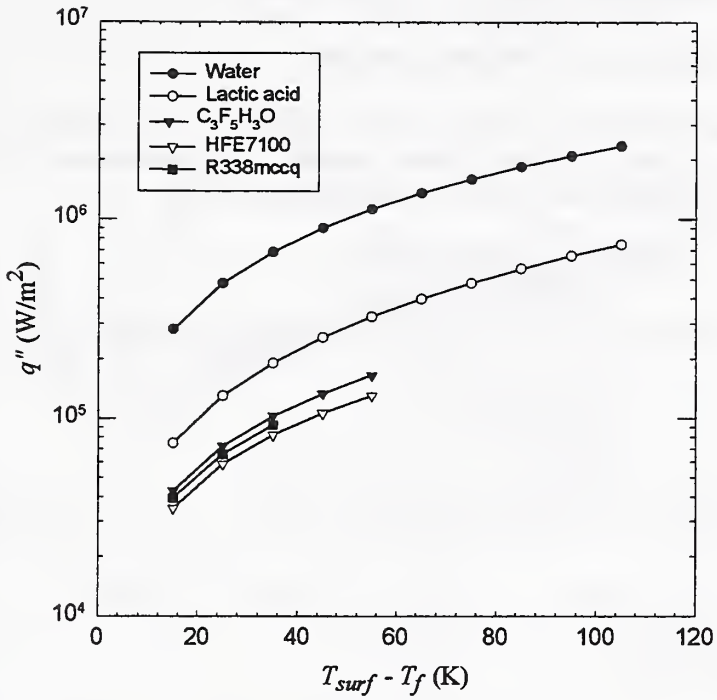

Figure 35. Calculated boiling curve in the convective regime.

removal from the surface in the nucleate boiling regime using these five liquids should be similar for a given T_{surf}.

F. Critical Heat Flux

The dimensionless correlation developed by Mudawar and Valentine [94] for water spray cooling over a wide range of flow rates is used to estimate the critical heat flux (*CHF*),

$$\frac{CHF}{\rho_g L Q''} = 122.4 \left\{ 1 + 0.0118 \left[\frac{\rho_g}{\rho_F} \right]^{1/4} \left[\frac{\rho_F C_{pf} (T_{sat} - T_f)}{\rho_g L} \right] \right\} \left(\frac{\sigma_f}{\rho_F Q''^2 D_{32}} \right)^{0.198} , \quad (33)$$

where ρ_g is the vapor density of the fluid, T_{sat} is the saturation temperature of the fluid, and σ_f is the surface tension of the fluid. All the fluid properties are evaluated at the fluid saturation temperature.

Using Q'' = 0.005 m^3/m^2-s, T_f = 295 K, and D_{32} = 0.5 mm, the resulting *CHF*s for water, lactic acid, $C_3F_5H_3O$, HFE7100, and R338mccq are 0.63 x 10^7 W/m^2, 0.86 x 10^7 W/m^2, 0.33 x 10^7 W/m^2, 0.23 x 10^7 W/m^2, and 0.21 x 10^7 W/m^2, respectively. In the calculations, surface tensions of water and lactic acid were obtained from the DIPPR [1]; while those of $C_3F_5H_3O$, HFE7100, and R338mccq were estimated using the method of Brock and Bird. [105] Although lactic acid and water have the highest and second highest *CHF*s, respectively,

under the conditions used in the calculations, it should be noted that it is inappropriate to compare the *CHF*s unless they occur at the same surface temperature for the five fluids, a situation highly unlikely given the differences in the thermophysical properties of these fluids.

G. Transition and Film Boiling Regimes

Based on dimensional analysis, Deb and Yao [108] statistically derived an equation for heat transfer effectiveness (ε) in terms of droplet Weber number (*We*), dimensionless wall superheat (B_w) and vapor parameters (K_d), and surface factor (*SF*) for surface material effect,

$$\varepsilon = 0.027 \exp\left[\frac{0.08\sqrt{\ln\left(\frac{We}{35}+1\right)}}{\left(B_w + \frac{SF}{60.5}\right)^{1.5}}\right] + 0.21 K_d B_w \exp\left[-\frac{90}{We+1}\right], \qquad (34)$$

with $We = \dfrac{\rho_F V_i D_o}{\sigma_f}$, $B_w = \dfrac{C_{pF}\left(T_{surf} - T_{sat}\right)}{L}$, $K_d = \dfrac{k_F}{C_{pF}\,\mu_v}$, and

$$SF = \sqrt{\frac{k_s \rho_s C_{ps}}{\left(k \rho C_p\right)_{steel}}} - 1 \quad ,$$

where V_i is the droplet impact velocity, K_d is the dimensionless vapor parameter, μ_v is vapor viscosity, and k_s, ρ_s, and C_{ps} are the thermal conductivity, density, and heat capacity of the surface material, respectively. All liquid and vapor properties are evaluated at T_{sat}. The heat transfer effectiveness is defined as the ratio of actual heat transfer from the hot surface to the total heat transfer required for complete evaporation of the droplets.; therefore, the heat flux from the surface is

$$q'' = \varepsilon G [L + C_{pf} (T_{sat} - T_f)], \qquad (35)$$

where G is the liquid mass flux. Equation (34) was obtained by fitting data mainly from experiments using a single stream of droplets. The experimental conditions covered the film boiling regime and to some extent the adjacent transition boiling regime and Leidenfrost point.

Figure 36 shows the calculated heat fluxes for the five fluids as a function of the surface temperature. The calculations were performed using T_f = 295 K, V_i = 2.5 m/s, D_o = 0.3 mm, and G = 0.5 kg/m^2-s. For illustration, a stainless steel, SS 304, was used as the target surface. Under the conditions used in the calculations, the resulting droplet *We* numbers are 31, 97, 181, 297, and 339 for water, lactic acid, $C_3F_5H_3O$, HFE7100, and R338mccq, respectively. The range of surface temperatures used in the calculations was chosen so that the calculated ε did not exceed 1. The three boiling regimes (transition boiling, Leidenfrost condition, and film boiling) are apparent in Figure 36. If we assume that at $T_{surf} \geq 800$ K, all five fluids exhibit film boiling, and lactic acid has the highest surface heat flux.

Figure 36 also demonstrates again the difficulty in comparing the heat fluxes at a given surface temperature. For example, at T_{surf} = 550 K, $C_3F_5H_3O$, HFE7100, and R338mccq are in the film boiling regime, whereas, water and lactic acid are in the transition boiling regime. As stated above, unless the surface temperature at

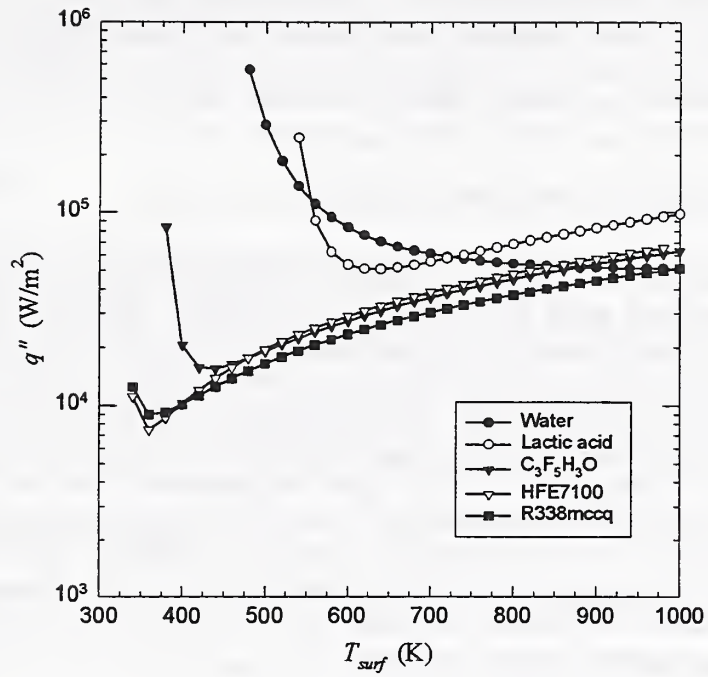

Figure 36. Calculated boiling curve in the transition and film boiling regimes.

which the onset of a particular boiling regime is known *a priori*, it is not possible to know which heat flux correlation pertaining to which boiling regime should be applied in the estimation.

H. Summary and Concluding Remarks

Empirical heat transfer correlations from the literature have been used to assess surface cooling in various heat transfer regimes. Based on the above calculations, *water* and *lactic acid* generally appear to be superior to $C_3F_5H_3O$, HFE7100, and R338mccq in *surface cooling* applications. Water and lactic acid evaporate much slower than $C_3F_5H_3O$, HFE7100, and R338mccq; therefore, the likelihood for water and lactic acid droplets to reach the surface is higher. For the convective boiling regime, the calculations show that water is better than lactic acid, $C_3F_5H_3O$, HFE7100, and R338mccq. Lactic acid has the highest calculated critical heat flux as well as the highest heat flux in the film boiling regime. In order to validate the calculated ranking of surface cooling effectiveness of these agents, experiments should be performed in various heat transfer regimes under conditions commensurate with those in actual applications.

Surface cooling by liquid droplets is a very complicated heat transfer process because it depends on so many parameters which include the thermophysical properties (surface tension, density, viscosity, heat of vaporization, etc.) of the liquid, droplet size, droplet impact velocity, spray mass flux, and surface properties. Even for non-burning, smooth surfaces, calculations of surface heat fluxes from first principles are not possible without resorting to experimental observations. Empirical heat transfer correlations under conditions encountered in fires are lacking, and the quantification of surface cooling as a means to extinguish the burning fuel remains elusive, especially when the fuel is a liquid.

In order to obtain a better understanding of droplet cooling of solid surfaces during fires, experiments performed under the conditions (droplet size, momentum, application rate, etc.) encountered in fire fighting are needed in the various heat transfer regimes. These types of experiments are still lacking in the literature. Surface cooling experiments involving liquid droplets and liquid surfaces are non-existent because the complexity of droplet-surface interaction makes the characterization of the heat transfer processes very difficult. A significant experimental effort in this area will be necessary to develop the knowledge and engineering correlations required for fire-fighting applications

V. RECOMMENDATIONS FOR ADDITIONAL STUDY

The current investigation has provided significant new insights into the behavior and desired characteristics of fire extinguishing agents which act purely by heat extraction. All three of the major components have indicated that such agents can have efficiencies in terms of volume or mass requirements which, while reduced from those of halon 1301, whose production have been banned., are sufficiently high to warrant further investigation as possible replacements. Recommendations are provided here for a limited research effort designed to provide additional understanding of thermal agent behavior and characteristics and to provide experimental results for one potential thermal agent, methoxy-nonafluorobutane, which appears promising and for which only limited experimental results are available. The survey of data bases indicated that lactic acid has physical properties which should make it a particularly effective fire extinguishing agent. Due to it corrosiveness, lactic acid alone is unlikely to be used for this purpose. However, it is possible that a useful agent could be made by mixing lactic acid with water. For this reason, the effectiveness of water/lactic acid mixtures for fire extinguishing will also be tested.

One of the gaps in knowledge for the current investigation was the lack of experimental measurements of extinguishment concentrations for gaseous thermal agents in methane/air diffusion flames. We propose to use an existing coflowing burner to measure extinguishing concentrations for N_2, Ar, He, and CO_2. If successful, this approach will provide an easily implemented, alternate approach for experimentally characterizing the effectiveness of gaseous fire-extinguishing agents.

All of the detailed chemical-kinetic modeling to date has used methane as the fuel. It is important to investigate the sensitivity of the findings to the fuel used. A limited series of calculations will be performed for a more complicated fuel such as ethylene or heptane, and the results will be compared to those using methane in order to identify any effects of fuel on extinguishing behavior.

An important finding of the kinetic modeling was that the location of heat extraction is not important to the effectiveness of a thermal agent as long the resulting heat deficit is convected into the flame zone. Much of the heat extraction associated with the release of liquid agents such water or methoxy-nonafluorobutane can be due to evaporation of the liquid at ambient and raised temperatures as the liquid droplets travel to and enter flame zones. Most laboratory methods for testing fire extinguishing efficiency use only gases, so the contribution of the heat of vaporization is not exploited. A unique counterflow diffusion flame facility at NIST is designed to investigate the effectiveness of liquid agents released into an ambient air coflow. During the next funding period it is proposed that this facility be used to compare the effectiveness of methoxy-nonafluorobutane when released either as a gas or as a liquid. It is anticipated that the mass flow of this agent required to cause extinction of the counterflow flame for a given strain rate will be lower for the liquid. This experiment represents an important test of our understanding of the effectiveness of thermal agents. The findings of this experiment also have practical limitations for specifying the amount of an agent required to extinguish a fire and for the design of systems designed to deliver liquid agents.

VI. ACKNOWLEDGEMENTS

This research is part of the Department of Defense's Next Generation Program Fire Suppression Technology Program, funded in part by the DOD Strategic Environmental Research and Development Program under Contract W74RDV73243630.

VII. REFERENCES

1. *DIPPR Data Compilation of Pure Compound Properties Database*, V9.02, NIST Standard Reference Data Program #11, NIST, Gaithersburg MD (1995).
2. *NIST Thermodynamic Properties of Refrigerants and Refrigerant Mixtures Database (REFPROP)*, V5.0, NIST Standard Reference Data Program #23, NIST, Gaithersburg MD (1996), V6.0, (1998).
3. Heathfield, A. E., Anastasi, C., Pagsberg, P., and McCulloch, A., *Atmosph. Envir.* **32**, 711-717 1998.
4. Grzyll, L. R., Back, D. D., Ramos, C., and Samad, N.A., *Development of a Rapid Screening Technique for Second-Generation Halon Alternatives*, SBIR Phase II Final Report, Contract Number DAAH01-93-C-R150, (1996).
5. Minor, B., *Compositions Including a Three Carbon Cyclic Fluoroether*, U.S. Patent No. 5480572 (1996).
6. Minor, B., *Compositions Including a Fluoroamine and a Second Component*, U.S. Patent No. 5441659 (1995).
7. Minor, B., Chisolm, T. E. C., and Shealy, G. S., *Azeotrope (Like) Compositions with Fluoromethyl Trifluoromethyl Ether and Dimethyl Ether*, U.S. Patent No, 5607616 (1997).
8. Pitts, W. M., Nyden, M. R., Gann, R. G., Mallard, W. G. and Tsang, W., *Construction of an Exploratory List of Chemicals to Initiate the Search for Halon Alternatives*, NIST Technical Note 1279 (1990).
9. Sekiya, A. and Misaki, S., *Chemtech* **26**, 44-48 (1996).
10. NIST *Structures and Properties Database and Estimation Program*, NIST Standard Reference Data Program #25,Versoin 2.02, National Institute of Standards and Technology, Gaithersburg, MD (1994).
11. Fishtine, S. H., *Ind. Eng. Chem.* **55**, 20-28 (1963).
12. Hawley, G. G., *Condensed Chemical Dictionary, Eighth Ed.*, Van Nostrand Reinhold Company, New York (1971).
13. Chueh, C. F. and Swanson, A. C., *Chem. Eng. Progress* **69**, 83-85 (1973); *Can. J. Chem. Eng.* **51**, 596-600 (1973).
14. Rihani, D. N. and Doraiswamy, L. K., *Ind. Eng. Chem. Fund.* **4**, 17-21 (1965).
15. *NIST Chemistry Webbook*, http://webbook.nist.gov.
16. 3M Corporation; web site http://www.mmm.com/fluids/7100.html.
17. Salvi-Narkhede, M., Adcock, J. L., Gakh, A., and Van Hook, W. A., *J. Chem. Thermodynamics* **25**, 643-647 (1993).
18. Wang, B. H., Adcock, J. L., Mathur, S. B., and Van Hook, W. A., *J. Chem. Thermodynamics* **3**, 699-710 (1991).
19. Matsuo, S., Tanaka, Y., Takada, N., Yamamoto, H., and Sekiya, A., *J. Chem. Eng. Data* **43**, 473-476 (1998).
20. Defibaugh, D. R., Carillo-Nava, E., Hurly, J. J., Moldover, M. R., Schmidt, J. W., and Weber, L. A., *J. Chem. Eng. Data* **42**, 488-496 (1997).
21. *Aldrich Fluorinated Products Catalog*, 1998-1999, Aldrich Chemical Company, Milwaukee, WI.
22. Defibaugh, D. R., Gillis, K. A., Moldover, M. R., Morrison, G., and Schmidt, J. W., *Fluid Phase Equilibria* **81**, 285-305 (1992).

23. Apollo Scientific, Derbyshire, UK; http://www.apolloscientific.co.uk/.
24. Peters, N., *Prog. Energy Combust. Sci.* **10**, 319-339 (1984).
25. Peters, N, *Twenty-First Symp. (Intl.) Combust.*, pp. 1231-1250, The Combustion Institute, Pittsburgh, (1986).
26. Tsuji, H., *Prog. Energy Combust. Sci.* **8**, 93-119 (1982).
27. Dixon-Lewis, G., *Twenty-Third Symp. (Intl.) Combust.*, pp. 305-324, The Combustion Institute, Pittsburgh (1990).
28. Potter, Jr., A. E., Heimel, S., and Butler, J. N., *Eighth Symp. (Intl.) Combust.*, pp. 1027-1034, Williams and Wilkins, Baltimore (1962).
29. Friedman, R. and Levy, J. B., *Combust. Flame* **7**, 195-201 (1963).
30. Ibiricu, M. M. and Gaydon, A. G., *Combust. Flame* **19**, 51-62 (1964).
31. Dodding, R. A., Simmons, R. F., and Stephens, A., *Combust. Flame* **15**, 313-315 (1970).
32. Milne, T. A., Green, C. L., and Benson, D. K., *Combust. Flame* **15**, 255-263 (1970).
33. Papas, P., Fleming, J. W., and Sheinson, R. S., *Twenty-Sixth Symp. (Intl.) Combust.*, pp. 1405-1411, The Combustion Institute, Pittsburgh (1996).
34. Hahn, W. A. and Wendt, J. O. L., *Eighteenth Symp. (Intl.) Combust.*, pp. 121-131, The Combustion Institute, Pittsburgh (1981).
35. Dixon-Lewis, G., David, T., Gaskell, P. H., Fukutani, S., Jinno, H., Miller, J. A., Kee, R. J., Smooke, M. D., Peters, N., Effelsberg, E., Warnatz, J., and Behrendt, F., *Twentieth Symp. (Intl.) Combust.*, pp. 1893-1904, The Combustion Institute, Pittsburgh (1984).
36. Smooke, M. D., Puri, I. K., and Seshadri, K., *Twenty-First Symp. (Intl.) Combust.*, pp. 1783-1792, The Combustion Institute, Pittsburgh, (1986).
37. Dixon-Lewis, G., David, T., and Gaskell, P. H., *Archivum Combustionis* **6**, 3 - 21 (1986).
38. Puri, I. K., Seshadri, K., Smooke, M. D., and Keyes, D. E., *Combust. Sci. Tech.* **56**, 1-22 (1987).
39. Chelliah, H. K., Law, C. K., Ueda, T., Smooke, M. D., and Williams, F. A., *Twenty-Third Symp. (Intl.) Combust.*, pp. 503-511, The Combustion Institute, Pittsburgh (1990).
40. Law, C. K., *Twenty-Second Symp. (Intl.) Combustion*, pp. 1381-1402, The Combustion Institute, Pittsburgh (1988)
41. Tsuji, H. and Yamaoka, I. *Twelfth Symp. (Intl.) Combust.*, pp. 997-1005, The Combustion Institute, Pittsburgh (1969).
42. Tsuji, H. and Yamaoka, I., *Thirteenth Symp. (Intl.) Combust.*, pp. 723-731, The Combustion Institute, Pittsburgh (1971).
43. Kee, R. J., Miller, J. A., Evans, G. H., and Dixon-Lewis, G., *Twenty-Second Symp. (Intl.) Combust.*, pp. 1479-1494, The Combustion Institute, Pittsburgh (1988).
44. Seshadri, K. and Williams, F. A., *Int. J. Heat Mass Transfer* **21**, 251-253 (1978).
45. Fisher, E. M., Williams, B. A., and Fleming, J. W., "Determination of the Strain in Counterflow Diffusion Flames From Flow Conditions," *1997 Fall Technical Meeting of the Eastern States Section of the Combustion Institute*, pp. 191-194, Hartford, CT (Oct. 27-29, 1997).
46. Maruta, K., Yoshida, M., Guo, H., Ju, Y., and Niioka, T., *Combust. Flame* **112**, 181-187 (1998).
47. Chan, S. H., Yin, J. Q., and Shi, B. J., *Combust. Flame* **112**, 445-456 (1998).
48. Gore, J. P., Lim, J., Takeno, T., and Zhu, X. L., Paper AJTE99-6311, Proceedings of the 5th ASME/JSME Joint Thermal Engineering Conference, San Diego, CA (March 15-19, 1999).
49. Westbrook, C. K., *Combust. Science Tech.* **23**, 191-202 (1980).
50. Westbrook, C. K., *Nineteenth Symp. (Intl.) Combust.*, pp. 127-141, The Combustion Institute, Pittsburgh (1982).
51. Westbrook, C. K., *Combust. Science Tech.* **34**, 201-225 (1983).
52. Noto, T., Babushok, V., Hamins, A., and Tsang, W., *Combust. Flame* **112**, 147-160 (1998).

53. Linteris, G. T., Burgess, Jr., D. R., Babushok, V., Zachaariah, M., Tsang, W., and Westmoreland, P., *Combust. Flame* **113**, 164-180 (1998).
54. Saso, Y., Zhu, D. L., Wang, H., Law, C. K., and Saito, N., *Combust. Flame* **114**, 457-468 (1998).
55. Rumminger, M. D., Reinelt, D., Babushok, V., and Linteris, G. T., *Combust. Flame* **116**, 207-219 (1999),
56. Hamins, A., Trees, D., Seshadri, K., and Chelliah, H. K., *Combust. Flame* **99**, 231-239 (1994).
57. Tanoff, M. A., Dobbins, R. R., Smooke, M. D., Burgess, Jr., D. R., Zachariah, M. R., and Tsang, W., "C_1 and C_2 Fluorinated Hydrocarbon Effects on the Extinction Characteristics of Methane Vs. Air Counterflow Diffusion Flames," pp. 116-126, *Halon Options Technical Working Conference*, Albuquerque, NM (May 6-8, 1997).
58. Lentati, A. M. and Chelliah, H. K., *Combust. Flame* **115**, 158-179 (1998).
59. Lentati, A. M. and Chelliah, H. K., *Twenty-Seventh Symp. (Intl.) Combust.*, pp. 2839-2846, The Combustion Institute, Pittsburgh (1998).
60. Tuovinen, H., *The Computer Modelling of the Combustion and Extinction of Methane-Air Premixed Flame, By Thermally Stable Gase*, SP Report 1989:54, Swedish National Testing Institution, Borås, Sweden (1989).
61. Lutz, A. E., Kee, R. J., Grcar, J. F., and Rupley, F. M., *OPPDIF: A Fortran Program for Computing Opposed-Flow Diffusion Flames*, SAND96-8243, Sandia National Laboratories, Livermore, CA (1996).
62. Kee, R. J., Rupley, F. M., Meeks, E., and Miller, J. A., *CHEMKIN-III: A FORTRAN Chemical Kinetics Package for the Analysis of Gas-Phase Chemical and Plasma Kinetics*, SAND96-8216, Sandia National Laboratories, Livermore, CA (1996).
63. Frenklach, M., Wang, H., Yu, C.-L., Goldenberg, M., Bowman, C. T., Hanson, R. K., Davidson, D. F., Chang, E. J., Smith, G. P., Golden, D. M., Gardiner, W. C., and Lissianski, V., *GRI-MECH 1.2*, http://www.me.berkeley.edu/gri_mech/
64. Fendell, F. E., *J. Fluid Mech.* **21**, 281-303 (1965).
65. Liñán, A., *Acta Astronautica* **1**, 1007-1039 (1974).
66. Giovangigli, V. and Smooke, M. D., *Combust. Science Tech.* **53**, 23-49 (1987).
67. Nishioka, M. and Law, C. K., *Combust. Flame* **104**, 328-342 (1996).
68. Norton, T. S., Smyth, K. C., Miller, J. H., and Smooke, M. D., *Combust. Science Technol.* **90**, 1-34 (1993).
69. Puri, I. K. and Seshadri, K., *Combust. Flame* **65**, 137-150 (1986).
70. Du, J. and Axelbaum, R. L., *Twenty-Sixth Symp. (Intl.) Combust.*, pp. 1137-1142, The Combustion Institute, Pittsburgh (1996).
71. Simmons, R. F. and Wolfhard, H. G., *Combust. Flame* **1**, 155-161 (1957).
72. Ishizuka, S. and Tsuji, H., *Eighteenth Symp. (Intl.) Combust.*, pp. 695-703, The Combustion Institute, Pittsburgh (1981).
73. Sheinson, R. S., Penner-Hahn, J. E., and Indritz, D., *Fire Safety J.* **15**, 437-450 (1989).
74. Roberts, A. F. and Quince, B. W., *Combust. Flame* **20**, 245-251 (1973).
75. Babb, M., Gollahalli, S. R., and Sliepcevich, C. M., *J. Propulsion Power* **15**, 260-265 (1999).
76. Hamins, A., Trees, D., Seshadri, K., and Chelliah, H. K, *Combust. Flame* **99**, 221-230 (1994).
77. Hamins, A., Gmurczyk, G., Grosshandler, W., Rehwoldt, R. G., Vazquez, I., Cleary, T., Presser, C., and Seshadri, K., "4. Flame Suppression Effectiveness," in *Evaluation of Alternative In-Flight Fire Suppressants for Full-Scale Testing in Simulated Aircraft Engine Nacelles and Dry Bays* (Grosshandler, W. L., Gann, R. G., and Pitts, W. M., Eds.), NIST SP 861, pp. 345-465, National Institute of Standards and Technology, Gaithersburg, MD (April, 1994).
78. Moore, T. A., Weitz, C. A., and Tapscott, R. E., "An Update of NMERI Cup-Burner Test Results," pp. 551-564, *Halon Options Technical Working Conference*, Albuquerque, NM (May 7-9, 1996).

79. Coward, H. F. and Hartwell, F. J., *J. Chem. Soc.*, 1522-1532 (1926).
80. Liñán, A. and Williams, F. A., *Fundamental Aspects of Combustion,* Oxford University Press, New York (1993).
81. Gordon, A. S., Smith, S. R., and McNesby, J. R., *Seventh Symp. (Intl.) Combust.*, pp. 317-324, Butterworths, London (1959).
82. Tapscott, R. E., Personal Communication, February 26, 1999, *NMERI In-House Testing*, June 2, 1997.
83. Flynn, R. M. and Thomas, S. D., *Fire Extinguishing Process and Composition*, U. S. Patent 5,718,293, February 17, 1998.
84. Downie, B., Polymeropoulos, C., and Gogos, G., *Fire Safety J.* **24**, 359-381 (1995).
85. Engel, O. G., *J. Res. NBS* **54**, 281-298 (1955).
86. Chandra, S. and Avedisian, C. T., *Proc. R. Soc. Lond.* **A432**, 13-41 (1991).
87. Chandra, S. and Avedisian, C. T., *Int. J. Heat Mass Transfer* **35**, 2377-2388 (1992).
88. Mundo, C., Sommerfeld, M., and Tropea, C., *Int. J. Multiphase Flow* **21**, 151-173 (1995).
89. Yarin, A. L. and Weiss, D. A., *J. Fluid Mech.* **283**, 141-173 (1995).
90. Bernardin, J. D. and Mudawar, I., *Int. J. Heat Mass Transfer* **39**, 2023-2037 (1996).
91. Bernardin, J. D., Stebbins, C. J., and Mudawar, I., *Int. J. Heat Mass Transfer* **40**, 73-88 (1997).
92. Bernardin, J. D., Stebbins, C. J., and Mudawar, I., *Int. J. Heat Mass Transfer* **40**, 247-267 (1997).
93. Bernardin, J. D. and Mudawar, I., *Int. J. Heat Mass Transfer* **40**, 2579-2593 (1997).
94. Mudawar, I. and Valentine, W. S., *J. Heat Treating* 7, 107-121 (1989).
95. Klinzing, W. P., Rozzi, J. C., and Mudawar, I., *J. Heat Treating* **9**, 91-103 (1992).
96. Mudawar, I. and Deiters, T. A., *Int. J. Heat Mass Transfer* **37**, 347-362 (1994).
97. Hall, D. D. and Mudawar, I., *Int. J. Heat Mass Transfer* **38**, 1201-1216 (1995).
98. Estes, K. A. and Mudawar, I., *Int. J. Heat Mass Transfer* **38**, 2985-2996 (1995).
99. Mudawar, I. and Estes, K. A., *ASME J. Heat Transfer*, **118**, 672-679 (1996).
100. Rein, M., *Fluid Dynamic Research* **12**, 61-93 (1993).
101. Henry, R. E. and Fauske, H. K., *ASME J. Heat Transfer* **101**, 280-287 (1979).
102. Spalding, D. B., *Some Fundamentals of Combustion*, Butterworths Scientific Publications, London (1955).
103. Kanury, A. M., *Introduction to Combustion Phenomena*, Gordon & Breach, New York (1975).
104. Chin, J. S. and Lefebvre, A. H., *AIAA J.* **21**, 1437-1443 (1983).
105. Reid, R. C., Prausnitz, J. M., and Poling, B. E., *The Properties of Gases & Liquids*, 4th ed., McGraw-Hill, New York (1987).
106. Lefebvre, A. H., *Atomization and Sprays*, Taylor & Francis, Washington (1989).
107. Qiao, Y. M., and Chandra, S., *ASME J. Heat Transfer* **120**, 92-98 (1998).
108. Deb, S. and Yao, S.-C., *Int. J. Heat Mass Transfer* **32**, 2099-2112 (1989).

U.S. Department of Commerce
National Institute of Standards and Technology

Manuscript Review and Approval

Attach Original of this Form to One Copy of Manuscript and Send to: WERB Secretariat, Mail Stop 2551 (NN/519)

(ERP Use Only - Version 2.10)

ERP Control Number	Division
Publications Report Number	Category Code
Publication Date	No. Printed Pages
[illegible]	Changes Permitted
7995	

Title and Subtitle (Cite in full)

Characterization and Identification of Super-Effective Thermal Fire Extinguishing Agents—First Annual Report

Author(s) (Last Name, First Initial, Second Initial)
Pitts, W M (Primary) ; Blevins, L G ; Huber, M L ; Yang, J C

Performing Organization:
NIST/GAITHERSBURG

Laboratory and Division
865 - Fire Science Division

Sponsoring Organization Name and Complete Address (Street, City, State, Zip)
DOD/SERDP,NIST

Type of Publication Proposed
NISTIR

Proposed for Non-NIST Publication (Cite fully)

Publishing Medium:
Paper

Abstract (A 2000-character or less factual summary of most significant information. If document includes a significant bibliography or literature survey, cite it here. Spell out acronyms on first reference.)

This report summarizes the first-year findings of a proposed three-year investigation of the feasibility of replacing halon fire-fighting agents with agents which act primarily by extracting heat from flame zones, i.e, thermal agents. Three distinct aspects of the effectiveness of potential thermal agents have been considered. First, existing thermodynamic databases maintained by NIST have been searched in order to identify chemical compounds which are predicted to extract large amounts of heat from a combustion zone. Second, detailed chemical kinetic modeling has been used to characterize the effects of thermal agents on an idealized flame system, namely, a methane/air counterflow diffusion flame. Third, empirical heat transfer correlations for spray cooling of a surface have been used to estimate the efficiencies of surface cooling by thermal agents. Recommendations are provided for the research effort during the second year of the project.

Supplementary Notes

Key Words (Maximum of 9; 28 characters and spaces each; Alphabetic order; Capitalize only proper names)

1. databases	**2. diluents**
3. diluent gases	**4. fire extinguishment**
5. fire extinguishing agents	**6. reaction kinetics**
7. surface cooling	**8. temperature effects**
9.	

Availability:

Unlimited

[illegible]

Announce Only After Publication:

Signature Page of MRA-OPS Form